Journal of Asian Earth Sciences 33 (2008) 414–427

Contents lists available at ScienceDirect

Journal of Asian Earth Sciences

journal homepage: www.elsevier.com/locate/jaes

Structural and geochronological constraints on the tectono-thermal evolution of the Danba domal terrane, eastern margin of the Tibetan plateau

Mei-Fu Zhou [a,*], Dan-Ping Yan [b], Paulo M. Vasconcelos [c], Jian-Wei Li [d], Rui-Zhong Hu [e]

[a] Department of Earth Sciences, University of Hong Kong, Hong Kong, China
[b] State Key Laboratory of Geological Processes and Mineral Resources, and School of Earth Sciences and Resources, China University of Geosciences, 29# Xueyuan Road, Beijing 100083, China
[c] Department of Earth Sciences, University of Queensland, Brisbane 4072, Australia
[d] State Key Laboratory of Geological Processes and Mineral Resources, and Faculty of Earth Resources, China University of Geosciences, Wuhan 430074, China
[e] Institute of Geochemistry, Chinese Academy of Sciences, Guiyang, China

ARTICLE INFO

Article history:
Received 16 December 2006
Received in revised form 2 March 2008
Accepted 17 March 2008

Keywords:
Eastern margin of the Tibetan plateau
Structure
Geochronology
Mantle plume
Post-orogenic extension

ABSTRACT

The Songpan-Ganze terrane of the Tibetan plateau is underlain by Neoproterozoic crystalline basement rocks of the Yangtze block. These basement rocks are exposed as a series of extensional tectonic domes that form a nearly north–south trending extensional belt more than 1000 km long in the eastern margin of the Tibetan plateau. In the Danba area, detachment faults separate the basement core complexes (e.g., the Gezong and Gongcai complexes) from the Paleozoic strata which have been thinned or removed completely. The cover sequences have undergone upper greenschist to lower amphibolite facies metamorphism to form the Danba schist and are overlain by the Triassic Xikang Group, a thick flysch sequence. Both the basement rocks and the Paleozoic rocks have undergone multiple stages of deformation and thus provide an excellent opportunity to study the tectono-thermal evolution of the eastern margin of the Tibetan plateau. Two stages of deformation, corresponding to three generations of foliation (S_1, S_2^1, and S_2^2), have been recognized on the basis of structural and microscopic observations. We selected amphibole and biotite separates associated with distinct generations of foliation for $^{40}Ar/^{39}Ar$ dating using laser microprobe incremental heating technique to place numerical constraints on the major tectono-thermal events within the Danba area. The geochronogical results reveal an earliest metamorphic event at 258.6 ± 0.5 Ma (S_1 biotite) and 263.6 ± 0.8 Ma (S_1 amphibole), coinciding temporally with the mantle plume that produced the voluminous Emeishan flood basalts. The second event was a progressive extensional deformation first occurred at 159–166 Ma (S_2^1 amphibole) responsible for the earlier tectonic doming of the crystalline basement, and then the final tectono-thermal overprint recorded by S_2^2 foliation and M_2^2 metamorphism locally in the core complexes at 47–58 Ma for the Gezong complex and 64–81 Ma for the Gongcai complex. This major post-orogenic extensional event is believed to be a consequence of collision between the North China and South China blocks. The apparent discrepancy of the $^{40}Ar/^{39}Ar$ ages observed between localities suggests a slow cooling process associated with progressive uplift.

1. Introduction

The tectonic evolution of the Tibetan plateau has been studied extensively over the past few decades (e.g., Yin and Harrison, 2000 and references therein). Such investigations have not only advanced our understanding of the genesis of the Himalayas and the development of the Tibetan plateau, but have extended our knowledge of the processes associated with uplift and exhumation of collisional orogens elsewhere. Studies of the eastern margin of the Tibetan plateau have documented multiple stages of deformation resulting from both the Cenozoic India-Eurasia collision, and the Mesozoic collision between the North China and South China blocks (e.g., Dirks et al., 1994; Burchfiel et al., 1995; Chen et al., 1995; Chen and Wilson, 1996; Worley and Wilson, 1996; Arne et al., 1997; Kirby et al., 2002; Wallis et al., 2003; Roger et al., 2004). These studies demonstrated the prolonged and complex nature of deformation in the Longmenshan thrust belt, the easternmost part of the Tibetan plateau (Fig. 1), which took place from the Indosinian (~220 Ma) until the Quaternary.

Although there are a few structural and metamorphic studies of the Danba region, west of the Longmenshan belt (i.e., Zhou et al., 2002a; Huang et al., 2003a,b), the effect of the India-Eurasia collision and pre-Tertiary tectono-thermal events in the area is not well

* Corresponding author. Tel.: +86 10 82320225; fax: +86 10 82322176.
E-mail address: yandp@cugb.edu.cn (D.-P. Yan).

1367-9120/$ - see front matter © 2008 Elsevier Ltd. All rights reserved.
doi:10.1016/j.jseaes.2008.03.003

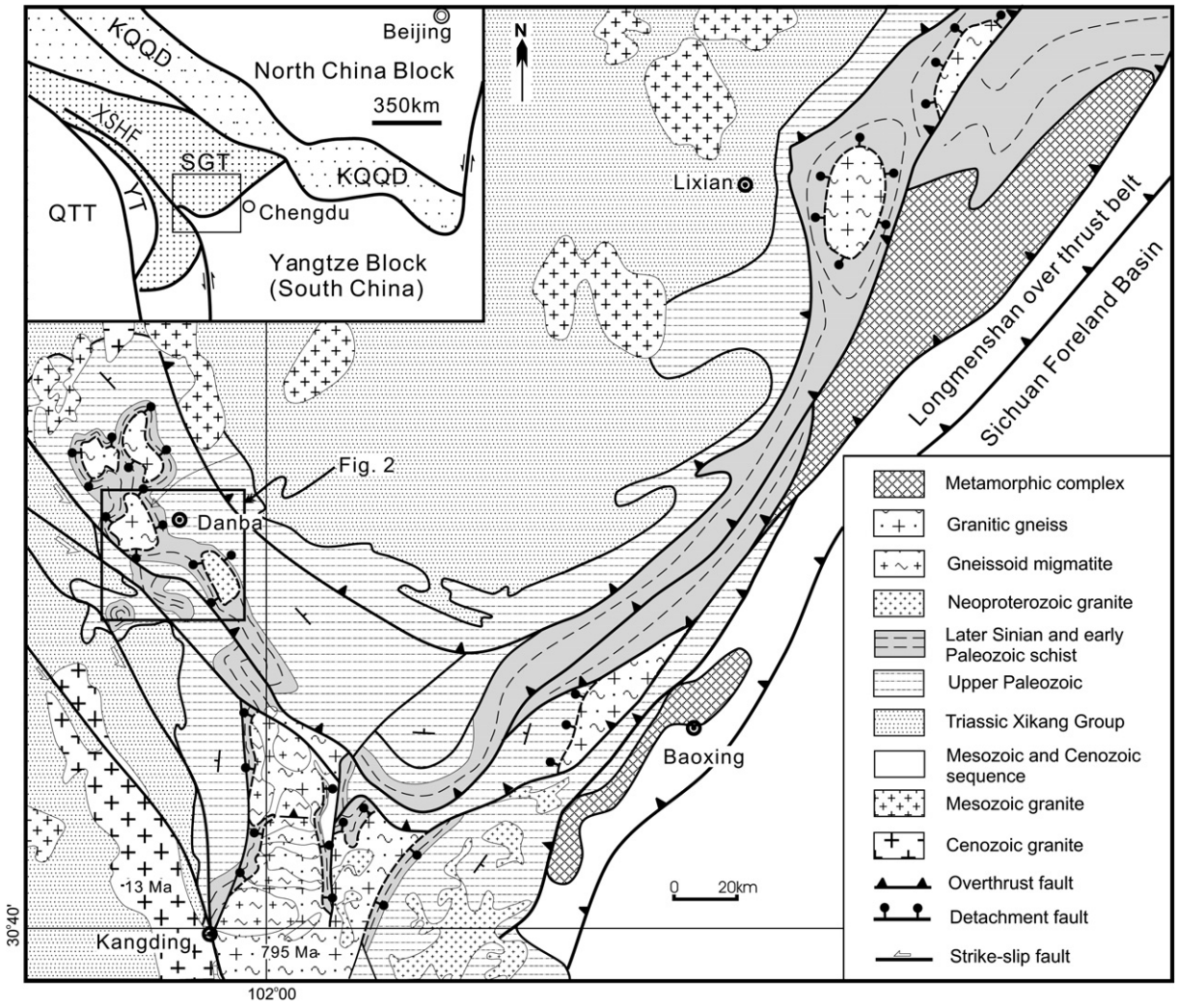

Fig. 1. Geological map of the Longmenshan and Danba areas along the western margin of the Yangtze block (modified from SBGMR, 1991); SGT, Songpan-Ganze terrane; KQQB, Kunlun–Qilian–Qinling–Dabie orogenic belt; YT, Yidun terrane; XSHF, Xianhuihe fault; QTT, Qiangtang terrane.

understood. It has been documented that tectonic domes form part of a nearly north–south trending extensional belt along this margin (Zhou et al., 2002a; Yan et al., 2003a), but timing of this tectonic event is unknown due to the lack of precise dating. The Permian Emeishan flood basalts record a voluminous volcanic event in the region (Chung and Jahn, 1995; Song et al., 2004), but its effects on the geology of the Danba area have not been previously documented.

In the Danba region, the metamorphosed Paleozoic assemblages within the Songpan-Ganze Triassic sequence are separated from several Neoproterozoic crystalline basement core complexes by detachment faults (Roger and Calassou, 1997; Zhou et al., 2002a; Huang et al., 2003a,b) [Figs. 1 and 2]. The Paleozoic sequences are in fault contact with the overlying Triassic sedimentary rocks, which experienced low-grade greenschist facies metamorphism. The variably metamorphosed assemblages from different crustal levels within this terrane have undergone multiple stages of deformation, providing an ideal opportunity to study thermal overprinting of the Paleozoic rocks and tectonic domes in relation to the tectonic events that have affected the region.

We carried out a mapping program in the Danba area over the past years and present here results of a detailed petrographic and $^{40}Ar/^{39}Ar$ geochronological study. Our new $^{40}Ar/^{39}Ar$ dates suggest that three major tectono-thermal events were recorded in the Danba domal terrane. These results provide important insights into the tectonic history of the eastern margin of the Tibetan plateau and into the tectonic relationship between the Yangtze block and the Tibetan plateau.

2. Geological background

The eastern margin of the Tibetan plateau is part of the Songpan-Ganze terrane, a Permo-Triassic mobile belt that stretches from the Pamir across the Kunlun Mountains into southwest China. This terrane is separated from the Kunlun–Qilian–Qinling–Dabie orogenic belt to the north by the Anyimaqen–Kunlun–Muztagh suture, from the Yangtze block to the east by the Longmenshan thrust belt (Fig. 1) (Dewey et al., 1988; Burchfiel et al., 1989; Chang, 2000; Yin and Harrison, 2000), and from the Yidun terrane by the Litang-Ganze suture to the south and southwest (Fig. 1). The Yangtze block consists of Paleoproterozoic to Neoproterozoic crystalline rocks overlain by a thick (>10 km) sequence of later Neoproterozoic (Sinian) to Cenozoic cover rocks. The crystalline rocks include paragneiss, mica–schist, graphite-bearing sillimanite–garnet gneiss (khondalite), amphibolite, marble, and quartzite. The cover sequences are composed of clastic, carbonate, and metavolcanic rocks (SBGMR, 1991; Mattauer et al., 1992; Xu et al., 1992; Yan et al., 2003b). Permian continental flood basalts (Emeishan basalts) crop out more than 2.5×10^5 km^2 in the region and are interpreted as the products of a mantle plume at 260 Ma (Chung and Jahn, 1995; Zhou et al., 2002c; Song et al., 2004).

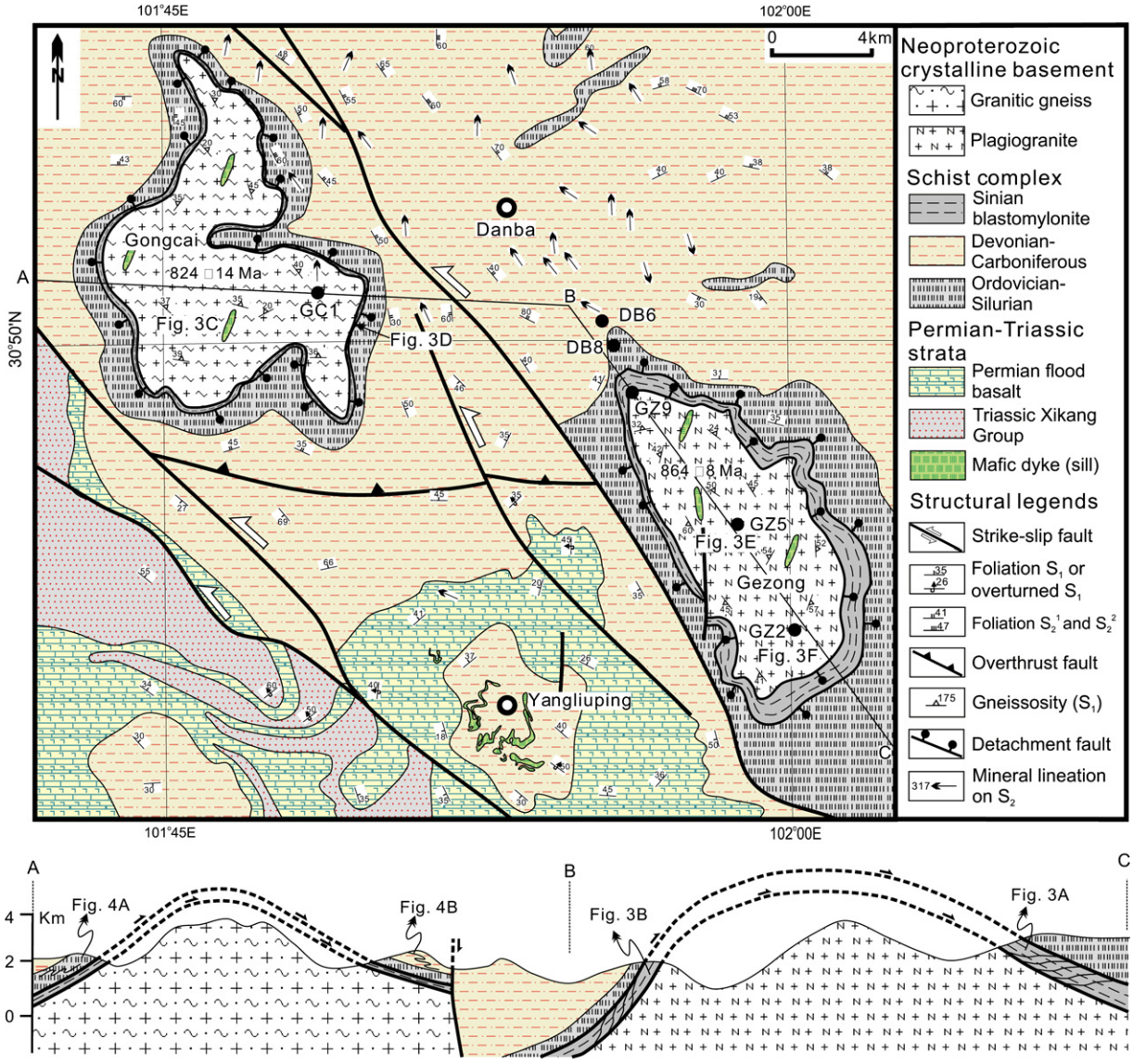

Fig. 2. Geological map of the Danba area, showing the distribution of metamorphic complexes and metamorphosed Paleozoic sequences (from Zhou et al., 2002a and our own field mapping).

A thick sequence (ca. 7 km) of Triassic marine strata forms the Xikang Group within the Songpan-Ganze terrane (Rao et al., 1987; Mattauer et al., 1992; Nie et al., 1994; Zhou and Graham, 1996; Bruguier et al., 1997; Chang, 2000). This sequence is attributed to a large flux of sediments from the Qinling–Dabie orogenic belt, which was created by the Triassic collision of the North China and South China blocks (Yin and Nie, 1993; Zhou and Graham, 1996).

In the eastern part of the Songpan-Ganze terrane, the Xikang Group is conformably underlain by Paleozoic shallow marine sequences of South China (Burchfiel et al., 1995). Several domes formerly interpreted as gneissic and structural domes or igneous core complexes (Hou, 1996; Roger and Calassou, 1997) are now considered to be typical of tectonic domes (see also Yin, 2004) formed by nearly east–west extension (Zhou et al., 2002a; Yan et al., 2003a). This interpretation is supported by significant stratigraphic omission or thinning of Sinian through Permian units around these domal structures (Fig. 2) (SBGMR, 1991).

The Longmenshan thrust belt forms the easternmost part of the Tibetan plateau and separates it from the Yangtze block (Liu et al., 1994; Burchfiel et al., 1995; Chen et al., 1995; Chen and Wilson, 1996; Worley and Wilson, 1996) [Fig. 1]. This thrust belt runs from NE to SW for more than 500 km. The Danba domal terrane is an extensional structure that occurs within a NW extension of the NE-trending Longmenshan belt (Fig. 1). It is likely that the NW-trending left-lateral Xianshuihe fault displaced this continuous belt. Clockwise rotation of the eastern part of the Songpan-Ganze terrane was associated with movement along this fault during the India-Eurasia collision (Chen et al., 1995; Arne et al., 1997; Worley and Wilson, 1996; Wang and Burchfiel, 2000), causing an overthrust of the Cenozoic Longmenshan fold belt onto the Sichuan basin, whereas the Danba portion was pushed toward the NW relative to the southern plate of the Xianshuihe fault (Fig. 1).

3. Geology of the Danba domal terrane

The Danba domal terrane consists of several Neoproterozoic crystalline basement core complexes, including the Gezong and Gongcai complexes and metamorphosed Sinian and Palaeozoic strata (referred to herein as the Danba schist). The core complexes are separated from the Danba schist by a major detachment fault and are interpreted as exhumed portions of the lower crust of the eastern margin of the Tibetan

plateau. The detachment faults around the core complexes are locally intruded by granites, which have been dated at 95–197 Ma (SBGMR, 1991; Roger et al., 2004). The Danba schist is overlain by the deformed Triassic Xikang Group, which is also intruded by numerous Mesozoic to Cenozoic granite plutons (Fig. 1).

3.1. Gezong and Gongcai basement complexes

The Gezong complex consists primarily of granite with lesser amounts of migmatite. The granite contains igneous zircons with a SHRIMP U–Pb age of 864 ± 8 Ma (Zhou et al., 2002a). The Gongcai complex is composed of migmatitic granites and gneisses which have an igneous precursor with a SHRIMP zircon U–Pb age of 824 ± 14 Ma (Zhou et al., 2002a).

Both complexes have domal shapes (Fig. 2) and are separated from the Sinian to Paleozoic schist sequence by detachment faults (Fig. 3A). Diabase and amphibolite dykes are abundant within the complex. Both complexes have experienced similar grades of metamorphism and deformation, as recorded in metamorphic mineral assemblages, foliations, and mineral lineations (Fig. 3A–F).

Two generations of foliation (S_1, S_2^1, and S_2^2) have been recognized in these complexes (Fig. 2). S_1 is a gneissic foliation defined by pervasive dark- and light-colored mineral bands (Fig. 3A–C). It is parallel to the bulk lithological layering and elongate lenses of relict amphibolite (S_0) (Fig. 3A and B). S_1 is well preserved, but was strongly superimposed by the subsequent foliations (S_2^1 or S_2^2), in particular along the detachment fault. S_2^1 is sub-parallel to S_1 with a small angle to S_0 (Fig. 3A and B) and forms a microscopic axial surface schistosity in macroscopic S_1 intrafolial folds. The S_2^1 foliation is mylonitic with S–C fabric (Fig. 3D) within the detachment fault, and is nearly parallel to it (Fig. 3A and B). The mineral lineations on the mylonitic foliation are oriented NNW–SSE (Fig. 2). S_2^2, only locally developed, is an EW-striking divisional cleavage. The S_2^2 cuts through the S_2^1 S–C fabric and has characteristics of ECC fabric, therefore, S_2^1 to S_2^2 indicates a progressive deformational process from deep to shallower tectonic level along the detachment fault.

The foliated rocks contain at least three different metamorphic assemblages (M_1, M_2^1, and M_2^2) [Fig. 3C–F]. M_1 is represented by biotite–(muscovite)–quartz–plagioclase, all of which are distributed along the S_1 foliation and occur as inclusions in other minerals (Fig. 3A and C). M_2^1 is a garnet–biotite–muscovite–quartz–plagioclase assemblage, which is distributed along the S_2^1 foliation (Fig. 3D–E) and reflects upper greenschist facies to lower amphibolite facies metamorphism. M_2^2 is characterized by a chlorite–biotite–muscovite–quartz assemblage, which occurs along the S_2^2 foliation (Fig. 3F) and represents lower greenschist facies metamorphism (Huang et al., 1996; Huang et al., 2003a). These three generations of metamorphism correspond to two stages of deformation (D_1 and D_2) under both extensional regimes. D_1 produced the S_1foliation and M_1 metamorphism; D_2 produced the S_2^1 foliation and M_2^1 metamorphism, and the S_2^2 foliation and M_2^2 metamorphism. D_1 represent an extensional deformation, while D_2 represent a progressive extensional deformation.

3.2. Danba schist

The Danba schist formed by upper greenschist to lower amphibolite facies metamorphism of Silurian–Devonian sedimentary strata. The major rock type is garnet–quartz–biotite–muscovite schist with local kyanite–quartz–muscovite schist, sillimanite–quartz–muscovite schist, and marble. Silurian strata locally underlie the Devonian rocks (SBGMR, 1991), but are considerably thinned by detachment faults within the schist complex.

All of these rocks exhibit a well-developed S_1 foliation sub-parallel to the detachment faults and to the original sedimentary layering (S_0) (Fig. 4A and B). S_1 foliation, which is defined by oriented micas (both biotite and muscovite) around porphyroblastic garnet and biotite, is discontinuous (Fig. 4C–F). The S_2^1 foliation, defined by metamorphic micas and quartz (Fig. 4C–E), is parallel to the detachment fault. S_2^2 is a cleavage similar to that of the complexes, and has a retrograde lower greenschist facies assemblage represented by randomly distributed minerals, such as biotite, muscovite, and chlorite (Fig. 4E and F).

4. Samples and analytical methods

Biotite and amphibole samples for $^{40}Ar/^{39}Ar$ dating were selected based on their field and textural relationships. Muscovite, although present in most samples, occurs generally as very fine-grained flakes and therefore was not considered for $^{40}Ar/^{39}Ar$ dating. After petrographic examination, mineral grains were carefully selected, washed in distilled water in an ultrasonic bath for 1 h, and dried. Five to ten grains of 1–2 mm from each sample were loaded into irradiation disks along with the Fish Canyon sanidine standards (28.02 ± 0.07 Ma; Renne et al., 1998). The disks were wrapped in Al-foil, vacuum sealed in silica glass tubes, and irradiated for 14 h at the B-1 CLICIT facility at the Radiation Centre, Oregon State University, USA. The sample and flux monitor irradiation geometries followed those of Vasconcelos (1999).

After a 3-month cooling period, we selected 2–3 grains from each sample for $^{40}Ar/^{39}Ar$ laser heating analysis. Heating with a laser beam (Innova 300 Ar-ion laser) defocused to 2 mm diameter permitted each grain to be heated nearly homogeneously, as confirmed by visual observation of grains through a video camera. Argon gases were extracted at consecutively higher laser powers lasting for 46–47 s at each designated laser power. The gases released during step heating were purified and then admitted into a MAP 215 mass spectrometer for argon isotopic analysis. Air pipettes and blanks were analyzed before and after each grain, yielding $^{40}Ar/^{36}Ar$ discrimination values ranging from 1.0145 ± 0.0018 to 1.0174 ± 0.0019. Full system blanks for ^{40}Ar range from 0.0005 ± 0.0000 to 0.0979 ± 0. 0013 nA (averaged at 0.0114 ± 0.0001) during the analysis, values considerably below the ^{40}Ar signals obtained for most gas fractions analyzed. All dates are calculated using $5.543 \times 10^{-10}\ a^{-1}$ as the total decay constant for ^{40}K (Steiger and Jager, 1977) and the following values for the reactor correction factors: $(2.64 \pm 0.02) \times 10^{-4}$ for $(^{36}Ar/^{37}Ar)_{Ca}$, $(7.04 \pm 0.06) \times 10^{-4}$ for $(^{39}Ar/^{37}Ar)_{Ca}$, and $(8 \pm 3) \times 10^{-4}$ for $(^{40}Ar/^{36}Ar)_{K}$.

5. $^{40}Ar/^{39}Ar$ analytical results

The analytical results are tabulated in Appendix, which will be made available in the journal's Data Repository. A summary of the $^{40}Ar/^{39}Ar$ ages is listed in Table 1. The corresponding apparent age spectra for samples are illustrated in Figs. 5–7. All dates reported were quoted at the 95% confidence level (2σ). In this study, an age plateau is defined as a sequence of two or more continuous steps that contain more than 50% of the total amount of ^{39}Ar released, and yield results reproducible at the 95% confidence level (2σ). A plateau-like (or pseudo plateau) spectrum is defined as a sequence of two or more contiguous steps containing more than 50% of the total ^{39}Ar released but the apparent ages of each step are slightly beyond the 95% confidence level (2σ) from the mean value.

5.1. Gezong complex

Both samples GZ-2 and GZ-9 contain larger biotite grains of S_2^2. Almost all amphibole in the sample GZ-5 belongs to S_2^1. Two biotite samples of S_2^2 foliation (GZ-2 and GZ-9) and one amphibole sample of S_2^1 foliation (GZ-5) were dated. Two biotite crystals from sample GZ-2 (Runs 1808-01 and 1808-02) yield

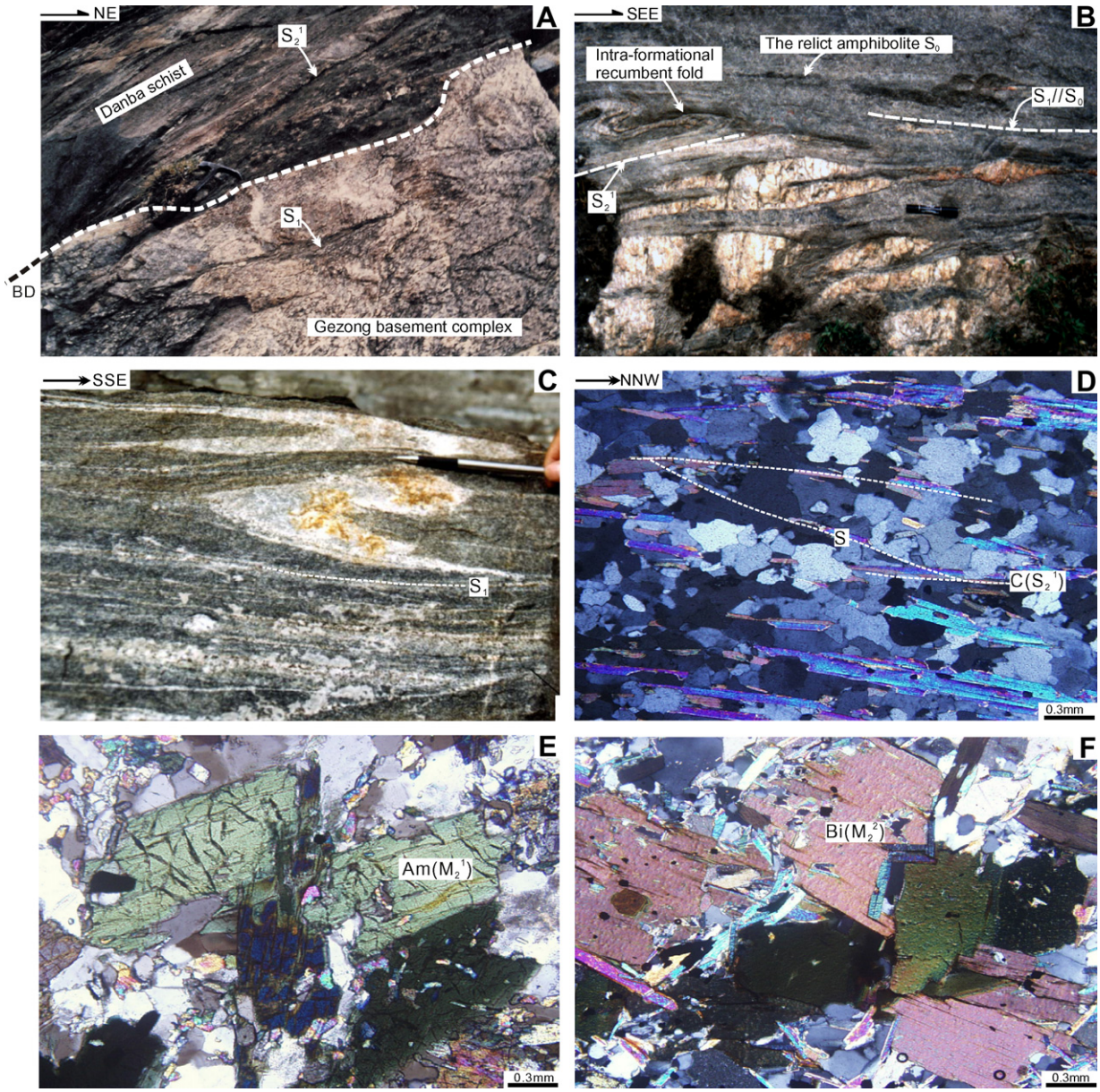

Fig. 3. Structural features of the basement core complexes and detachment fault of the Danba domal terrane, Western China. (A) Field photo of a ductile shear zone on top of the Gezong granitic complex showing a detachment fault (DF) between the Gezong basement complex and the Danba schist. Note that the mylonitic foliation S_2^1 is sub-parallel to the S_1 within the basement complex. (B) A ductile shear zone developed in the upper part of the Gezong complex showing the relationship among S_0, $S_1$and S_2^1. Note amphibolite, which shows the original S_0 foliation, is nearly parallel to the S_1 foliation, whereas S_2^1 is the axis of intra-formational recumbent folds of S_1 and has a small angle with S_1. Both S_1 and S_2^1 suggest an extensional feature of D_1 and D_2^1. (C) Gneissic S_1 within the Gongcai complex. The S_1 is the axis of S_0 intrafolial folds and is locally sub-parallel to the amphibolite band of probably S_0. (D) A microphotograph showing the S_2^1 foliation defined by elongate mica grains. The sample was collected from the detachment fault in the Gongcai complex. Note that the S–C fabrics indicate a SSE-ward shear sense. Sample location is shown in Fig. 2. (E) M_2 amphibole (Am) in a mafic dyke in the Gezong complex. (F) Large, undeformed biotite grains (Bi) formed during M_3 metamorphism in the Gezong basement complex.

well-defined plateau ages at 47.3 ± 1.8 and 58.3 ± 1.3 Ma (Fig. 5a and b), while the third grain (Run 1808-03) defines a plateau-like segment accounting for more than 90% of ^{39}Ar released, with a pseudo plateau age of 48 ± 3 Ma (Fig. 5c), which is reproducible with the plateau age of the first grain (Run 1808-01). However, the age of the second grain is distinct from those of other two grains.

Three biotite flakes from sample GZ-9 yield well-defined plateau ages ranging from 56.5 ± 0.5 to 51.2 ± 1.2 Ma (Fig. 5d and f). Plateau ages of the first and third grains (Runs 1814-01 and 1814-03) show remarkable reproducibility within errors (Fig. 5d and f), but they are 5 Mys. younger than the second grain (Run 1814-02; Fig. 5e). One amphibole grain (Run 1812-03) yielded a pseudo plateau age of 166 ± 9 Ma (Fig. 5g).

The integrated ages (equivalent to total fusion age) of each grain is in good agreement with the respective plateau ages (Fig. 5), suggesting that no excessive argon and mixture of phases occurred in these samples.

5.2. Gongcai complex

A granitic gneiss sample, GC-1, contains large biotite grains of S_2^2. Two of three biotite grains (Runs 1809-02 and 1809-03) yield well-developed plateau ages at 81.1 ± 0.4 and 64.8 ± 0.8 Ma, respectively (Fig. 6b and c). Heating of the third grain (Run 1809-01) produces a disturbed spectrum that did not reach a plateau (Fig. 6a). However, a pseudo plateau age can be obtained at 76.3 ± 0.9 Ma, defined by the middle to high temperature steps (steps C and D) that account

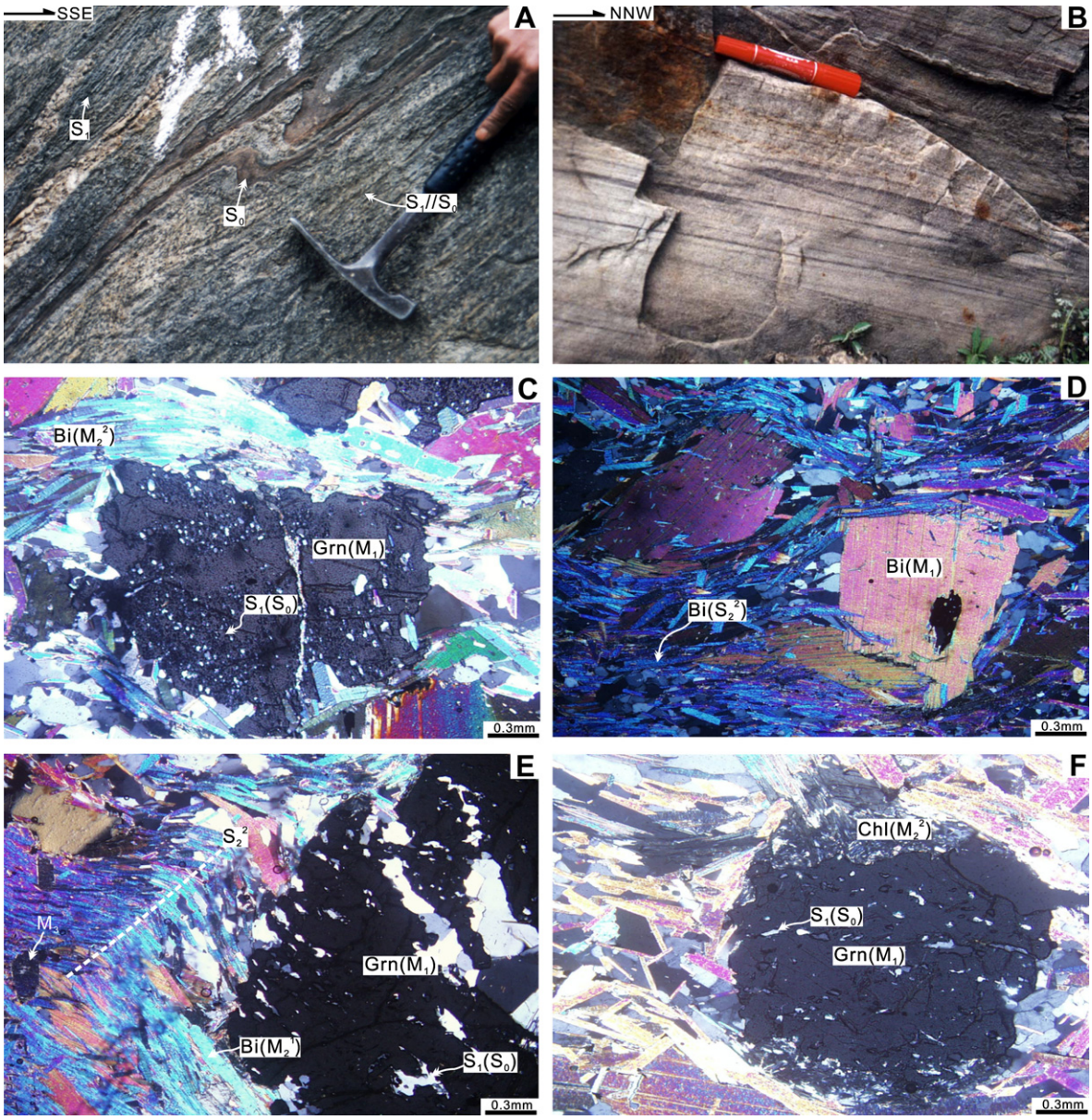

Fig. 4. Structural features of the Danba schist from the Danba domal terrane, Western China. (A and B) S_1 foliations are the axis of S_0 intra-formational recumbent folds and are sub-parallel to S_0. The locations are shown in the section of Fig. 2. (C) M_2^1 biotite (Bi) formed during D_2^1 deformation involving M_1 garnet (Grn). Note that S_1 foliations (sub-parallel to S_0) are preserved within the garnet. (D) M_2^1 biotite formed during D_2^1 deformation involving M_1 biotite. (E) S_2^2 Crenulation cleavage (ECC fabric) crosscuts S_2^1 and M_2^2 biotite crosscuts S_2^1 foliation and M_2^1 biotite. (F) A garnet porphyroblast (M_1) is surrounded by M_2^2 chlorite (Chl).

for ca. 40% of the amount of total ^{39}Ar released (Fig. 6a). The spectrum of this grain suggests partial argon loss from the minerals, as indicated by the slightly younger integrated ages relative to the corresponding plateau or pseudo plateau ages.

5.3. Danba schist

Two garnet mica schist samples, DB-8 and DB-6, consist mainly of S_1 biotite and amphibole. One of two biotite grains (Run 1815-01) from DB-8 yields a very well-defined plateau age of 258.6 ± 0.5 Ma and a comparable integrated age of 257.7 ± 0.4 Ma (Fig. 7a). The second grain (Run 1815-02) yields an ascending staircase spectrum characterized by very young apparent ages in the initial steps (Fig. 7b), indicative of post-formation argon loss. The integrated age of this biotite grain is 175.3 ± 0.4 Ma (Fig. 7b).

The first amphibole grain (Run 1816-01) from the mica schist sample, DB-6, yields a well-defined plateau age at 263.6 ± 0.8 Ma and an identical integrated age of 261.9 ± 0.4 Ma (Fig. 7c), which are slightly older than the biotite age for DB-8. The second grain (Run 1816-02) yields a plateau age at 159 ± 14 Ma with an integrated age of 272 ± 1 Ma (Fig. 7d). Relative large uncertainty in the plateau age is likely reflective of the very low radiogenic argon yield as indicated by the low K/Ca ratio of the mineral (Fig. 7d). The older integrated age of this grain (272 Ma) could be caused by a minor contamination by old phases, as revealed by the anomalously old apparent ages of the highest temperature steps (Fig. 7d).

6. Discussion

6.1. Evaluation of $^{40}Ar/^{39}Ar$ results

Most samples yield well-defined plateau ages (Figs. 5–7), suggesting absence of mixture of phases in our samples. This indicate

Table 1
Summary of $^{40}Ar/^{39}Ar$ ages of the Danba domal terrane

Sample	Grain ID#	Association	Plateau age (Ma)	±2σ (Ma)	Integrated age (Ma)	±2σ (Ma)
Biotite						
GZ-2	1808-01	S_3, M_3	47.3	1.8	47.9	1.1
	1808-02	S_3, M_3	58.3	1.3	57.9	0.9
	1808-03	S_3, M_3	48.0	3.0	51.6	1.6
GZ-9	1814-01	S_3, M_3	51.8	1.6	50.7	1.1
	1814-02	S_3, M_3	56.5	0.5	55.9	0.4
	1814-03	S_3, M_3	51.2	1.2	49.0	0.7
GC-1	1809-01	S_3, M_3	76.3[†]	0.9	70.7	0.4
	1809-02	S_3, M_3	81.1	0.4	79.53	0.18
	1809-03	S_3, M_3	64.8	0.8	63.3	0.4
DB-6	1815-01	S_1, M_1	258.6	0.5	257.7	0.4
	1815-02	S_1, M_1	N.A.	N.A.	175.3	0.4
Amphibole						
GZ-5	1812-03	S_2, M_2	166.0	9.0	194.0	5.0
DB-8	1816-01	S_1, M_1	263.6	0.8	261.9	0.4
	1816-02	S_1, M_1	159.0	14.0	272.0	1.0

N.A., Not applicable.
[†] Forced plateau age.

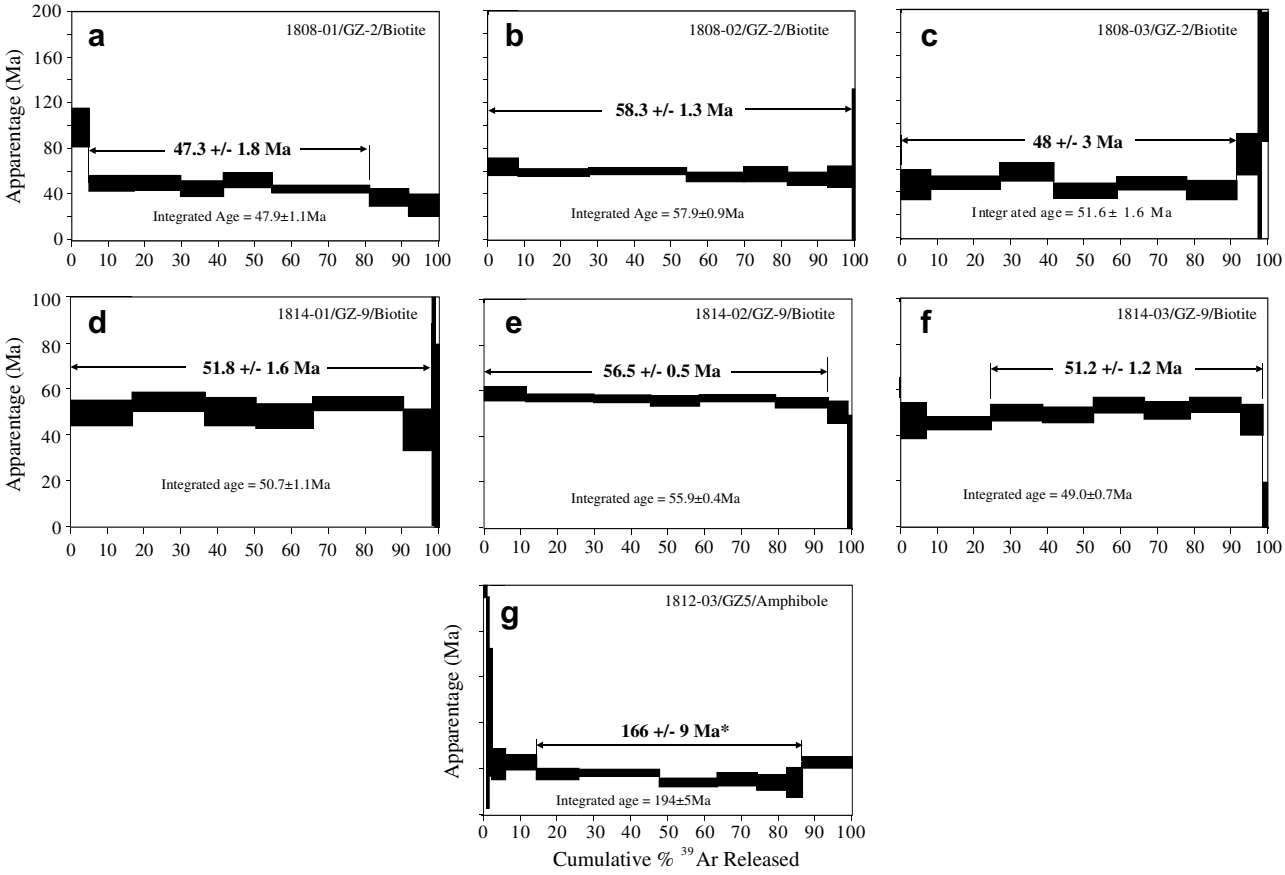

Fig. 5. $^{40}Ar/^{39}Ar$ spectra of biotite and amphibole separates from granites (GZ-2 and GZ-9) and amphibolite (GZ-5) in the Gezong complex of the Danba domal terrane, Western China.

that the present $^{40}Ar/^{39}Ar$ ages can be reliably interpreted as the cooling ages of the metamorphic biotite and amphibole at their closure temperatures, 300–350 and 500–550 °C, respectively (McDougall and Harrison, 1999). The consistence between plateau or plateau-like ages and integrated ages for most sample and reproducibility of $^{40}Ar/^{39}Ar$ plateau ages among distinct grains from the same sample (GZ-2, GZ-9, and GZ-5) further attest to the reliability of the present analyses. However, samples DB-6, DB-8, and GC-1 show distinct plateau ages among different grains (Figs. 6 and 7). We interpret such discrepancy as results of disturbance of the Early Triassic metamorphic rocks by later thermal events. Some grains are characterized by low apparent ages at the low temperatures, indicating partial argon loss caused by later thermal overprinting.

The $^{40}Ar/^{39}Ar$ ages can be gathered into three groups: (1) 259–264 Ma (M_1 biotite and amphibole); (2) 159–166 Ma ($M_2{}^1$ amphibole); and (3) 47–81 Ma ($M_2{}^2$ biotite). The age difference for the first group may simply reflect different closure temperature of

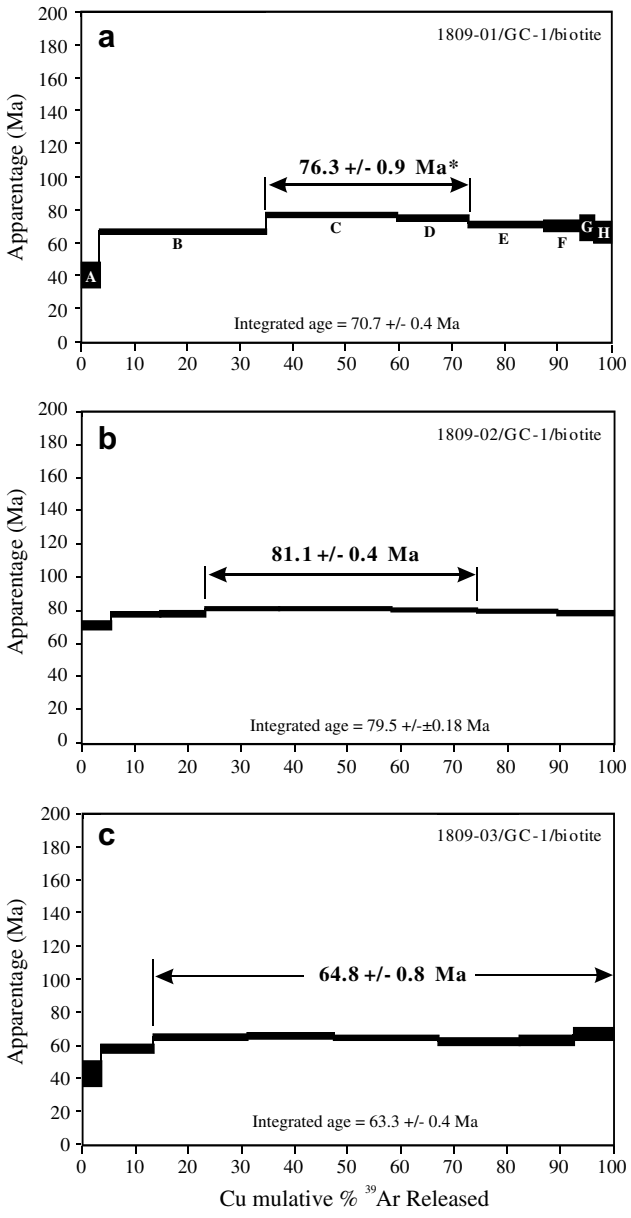

Fig. 6. $^{40}Ar/^{39}Ar$ spectra of biotite separates from a granitic gneiss (GC-1) in the Gongcai complex of the Danba domal terrane, Western China.

argon isotopes in biotite (300–350 °C) and amphibole (500–550 °C) (McDougall and Harrison, 1999). However, one amphibole grain from the M_1 metamorphic assemblage gave an apparently young age at 159 ± 14 Ma, which is broadly consistent with the second age group, and is interpreted in terms of thermal reset by a young tectono-thermal event represented by the second age group. Three amphibole $^{40}Ar/^{39}Ar$ ages from group 2 are identical within errors.

In the third group, biotite minerals from the Gezong and Gongcai complexes have cooling ages of 47–58 and 64–81 Ma, respectively. This group is characterized by apparent variation in the plateau age from grain to grain and from sample to sample. Such an age discrepancy may suggest that the Gezong and Gongcai complexes have been overprinted by a later thermal event that caused partial but uneven argon gas loss from the samples. However, existing studies provide no evidence for such a thermal event regionally. We therefore suggest that age variations may be more likely reflective of the effect of mineral grain size on the diffusion of argon isotope from the host minerals (Markley et al., 1998, 2002; Castonguay et al., 2001). It is well documented that diffusion loss of radiogenic argon during cooling is less significant in the larger grains and that these accordingly yield older ages (Wright et al., 1991; Cosca et al., 1992; Hess et al., 1993; West and Lux, 1993; Markley et al., 1998, 2002). The variable sizes of the M_3 biotite separates from Danba may explain the geochronological results with the older dates for the larger grains.

6.2. Thermal events in the Danba domal terrane

As described earlier, the present $^{40}Ar/^{39}Ar$ dates reveal three major thermal events in the Danba area since the late Paleozoic, which correspond to three stages of deformation and metamorphism. An early stage of metamorphism at 259–264 Ma was followed by a second stage of metamorphism from 159 to 166 Ma to a final phase of deformation between 47 and 81 Ma.

6.2.1. Metamorphism at 259–264 Ma

The Danba schist (M_1–D_1) was traditionally considered to have formed by Indosinian (~220 Ma) metamorphism, immediately after the collision between the South China and North China blocks. Age of the schist was originally constrained by Xia (1993) and Hou (1996) at 194–152 Ma using whole rock K–Ar and Rb–Sr dating methods. These are consistent with the emplacement ages of the granite intruded the Danba schist between 150 and 197 Ma (Roger et al., 2004). More recently, Huang et al. (2003b) obtained Rb–Sr and Sm–Nd ages on mineral separates between 204 and 190 Ma. They concluded that the metamorphism was associated with extensive magmatism within the Songpan-Ganze terrane. Our $^{40}Ar/^{39}Ar$ data provide new constraints on the formation and evolution of the Danba schist.

The Danba schist has a mineral assemblage (M_1) corresponding to lower amphibolite facies or upper greenschist facies metamorphism. The $^{40}Ar/^{39}Ar$ ages of 259–264 Ma yielded by the M_1 biotite and amphibole reflect the timing of this metamorphism, which is coeval with the magmatism of the Emeishan Large Igneous Province at 260 Ma (Zhou et al., 2002c; Guo et al., 2004). In the absence of any other known events of this age, it is inferred that this metamorphism was caused by pervasive underplating of mafic magmas, represented by the Emeishan volcanic sequences and feeder dykes. The Emeishan flood basalts are exposed over an area of more than 2.5×10^5 km^2 in the western part of the Yangtze block and eastern margin of the Tibetan plateau where they comprise the major part of the Permian strata (Fig. 2). In the Danba area, the widespread Permian flood basalts have been metamorphosed to greenschist facies during post-Permian thermal events (Song et al., 2004). There are numerous mafic dykes in the Danba schist that are believed to be feeders to the Emeishan flood basalts and related mafic–ultramafic sills in the Yangliuping area, south of Danba (Fig. 2), containing economic Ni–Cu–(PGE) sulfide deposits (Zhou et al., 2002b,c; Song et al., 2003, 2004).

It has been documented that the middle Permian mantle plume not only produced large volumes of mafic magmas but was also responsible for the doming and uplift of the lower crust (He et al., 2003). High-temperature metamorphism may have been associated with continental rifting or extension (e.g., Wichham and Oxburgh, 1985; Sandiford and Powell, 1986; Zen, 1995), or basaltic magma underplating (Collins and Vernon, 1994; Bodorkos et al., 2002; Schmitz and Bowring, 2003). Therefore, the 259–264 Ma deformation (D_1) for the Danba terrane reinforces the hypothesis of an anorogenic metamorphism associated with a mantle plume.

6.2.2. Post-orogenic progressive extension from 159–166 Ma to 47–81 Ma

The second stage of deformation (D_2) in Danba includes two phases: the first phase (D_2^1) at 159–166 Ma appears to be

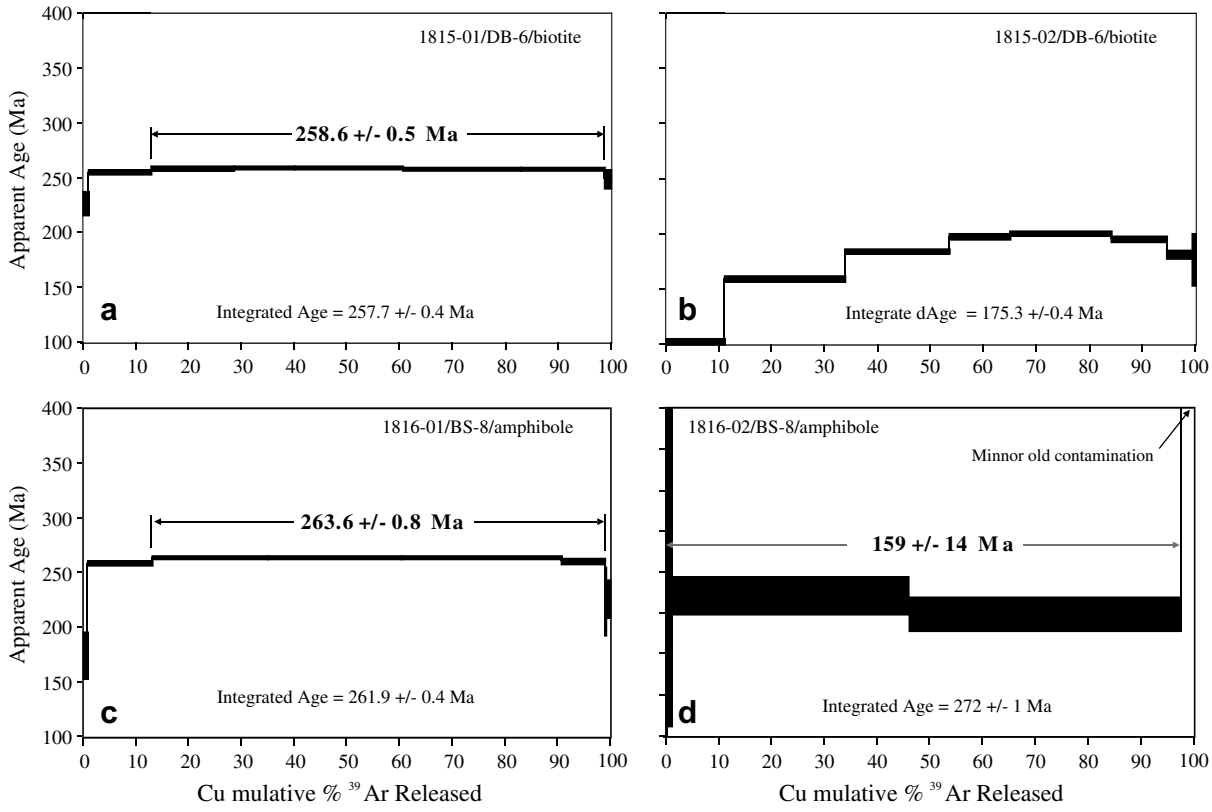

Fig. 7. $^{40}Ar/^{39}Ar$ spectra of biotite and amphibole separates from a garnet mica–schist (DB-6) and amphibolite (DB-8) in the Danba schist of the Danba domal terrane, Western China.

widespread in the western part of the Yangtze block. This phase is also recorded along the Longmenshan belt in the easternmost part of the Tibetan plateau (Wallis et al., 2003). The metamorphic ages are consistent with previous K–Ar dates on illite from the Xikang Group, which range from 152 to 177 Ma (SBGMR, 1991). Huang et al. (2003b) reported an age range of 168–158 Ma using a combination of U–Th–Pb monazite and titanite and Sm–Nd garnet ages. This phase of deformation is also recorded in the 177 Ma metamorphic rims over 860 Ma igneous zircons from the Gongcai complex (Zhou et al., 2002a). Many authors have reported a ca.170 Ma thermal overprint on the Emeishan flood basalts (Boven et al., 2002; Hou et al., 2002; Ali et al., 2004; Roger et al., 2004). These ages are believed to date the starting of a major extensional event, which led to domal uplift of the core complexes (Zhou et al., 2002a). The second phase (D_2[2]) is dated at 47–58 Ma using M_2[2] biotite separates from the Gezong complex and at 64–81 Ma from the Gongcai complex (Figs. 5 and 6). Similar ages have been obtained for the eastern margin of the Tibetan plateau by a number of researchers. Hou (1996) reported K–Ar and Rb–Sr ages of 80 Ma for muscovite and bulk rocks from pegmatites, whereas Xu et al. (1992) reported Rb–Sr whole rock ages of 62 Ma. Wallis et al. (2003) obtained a $^{40}Ar/^{39}Ar$ age of ca. 65 Ma. This group of ages resulted from a thermal event, and the age scatter possibly reflects a slow cooling rate.

Markley et al. (1998, 2002) noted that regional variations in deformation mechanisms affect the effective diffusion dimension (EDD) of mica, and that the EDD of mica is the grain size itself. Thus, regional thermal variations may have exerted a more direct control on the dates. According to diffusion theory (McDougall and Harrison, 1999), mica cooling ages should vary with grain size in a manner consistent with reasonable geological estimates of cooling rates. Mica grains subject to reheating should display a similar relationship between $^{40}Ar/^{39}Ar$ ages and grain size. In contrast, diffusion theory predicts that $^{40}Ar/^{39}Ar$ ages reflecting mica growth should not vary substantially with grain size. Therefore, the large age spread of biotite in the Gezong and Gongcai complexes suggests that the biotite was thermally reset during the 47–81 Ma event. The cooling rate of the core complexes following their emplacement may have been extremely slow for 25 million years.

6.3. Tectonic implications for the eastern margin of the Tibetan plateau

Earlier studies proposed that the thick Triassic Xikang Group along the eastern part of the Songpan-Ganze terrane was deposited on the continental basement of South China (e.g., Burchfiel et al., 1995). The presence of tectonic domes in the Danba area supports this interpretation, because they are similar to the basement complexes of the Yangtze block elsewhere (Zhou et al., 2002a; Yan et al., 2003a). This suggests that the eastern margin of the Tibetan plateau originally coincided with the Triassic western margin of the Yangtze block.

Our geochronological studies in the Danba terrane yield additional information about the core complexes and show that both the core complexes and the schist complex experienced multiple thermal histories. The schist complex as a cover sequence was metamorphosed at ca. 260 Ma, whereas the core complexes were largely affected by progressive extensional deformation from 168–173 to 47–81 Ma. Biotites from the cover sequence differ from the basement complexes, and such difference may be due to different temperature range for Ar-diffusion. The Danba terrane was characterized by spatial variations in uplift rates. From our new dataset, the tectonic processes in the region may be summarized as follows (Fig. 8).

The crystalline basement in the region was consolidated from a Neoproterozoic (750–860 Ma) arc assemblage, presently exposed in Gezong and Gongcai (Roger and Calassou, 1997; Zhou et al.,

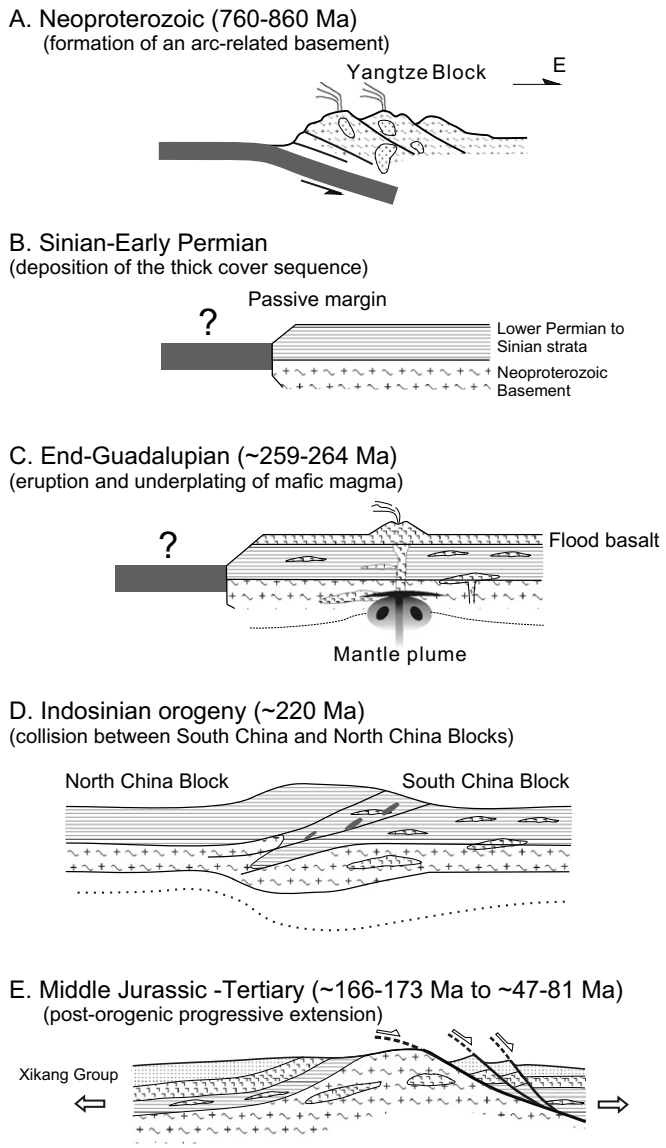

Fig. 8. A schematic model summarizing the tectono-thermal history of the Danba domal terrane, Western China.

2002a). During Neoproterozoic, South China, including the Yangtze and Cathaysia blocks, may have been part of the Rodinian supercontinent (Li et al., 1995; Zhang and Piper, 1997). Between the Late Neoproterozoic and the Ordovician, the South China block drifted away from East Gondwanaland and Laurentia toward North China. During this time it experienced rapid subsidence and was covered by a thick Late Sinian–Cambrian succession of platform carbonates, phosphorites, and black shales (Fig. 8A and B). At the end of the Guadalupian (ca. 260 Ma), a mantle plume reached the base of the crust along the western margin of the Yangtze block, leading to rapid and voluminous eruption to form the Emeishan flood basalts and intrusion of mafic sills and layered intrusions (Zhou et al., 2002c) [Fig. 8C]. Extensive underplating by mafic magma and continental extension caused lower amphibolite facies and upper greenschist facies metamorphism (M_1) of the Silurian to Devonian strata to form the Danba schist.

Following the Emeishan mantle plume in the Late Middle-Permian, South China continued drifting northward. Eventually collision between the North China and South China blocks began in east China at ca. 230 Ma and produced the ultra-high pressure Dabie-Sulu terrane (e.g., Li et al., 1993), coincident with rapid deposition in the Songpan-Ganze basin to form a thick Triassic sequence of the Xikang Group (Nie et al., 1994; Yin and Nie, 1993, 1996). South China continuously moved northward with a clockwise rotation and eventually collided with the Songpan-Ganze terrane, resulting in continued NE–SW shortening and in localized crustal thickening. The Xikang Group was intensely deformed by folding and thrusting during the Late Triassic and Early Jurassic (Chen et al., 1995; Burchfiel et al., 1995; Yin and Nie, 1996; Worley and Wilson, 1996) [Fig. 8].

Exhumation of the crystalline basement began with an originally nearly E–W extension (Zhou et al., 2002a; Yan et al., 2003a), if recovered from the Cenozoic rotation along the Xianshuihe sinistral fault (Wang and Burchfiel, 2000), although the present lineation points to a phase of NNW–SSE extension (Fig. 1). This extensional deformation thinned and locally removed the Paleozoic strata overlying the basement. It has also resulted in the uplift of the lower portion of the crust to form the Danba tectonic domal terrane. This event first occurred at 166–173 Ma and was associated with intrusion of post-orogenic I-type granites that are widespread in the Songpan-Ganze terrane (Fig. 8E). As a result of decompression melting, both the Gezong and Gongcai complexes experienced significant migmatization. The continuous deformation ($D_2{}^2$) in the Danba region suggests re-activation of the eastern part of the Songpan-Ganze terrane at 47–81 Ma (Fig. 8F). The age range of this thermal event at 47–81 Ma is older than the India-Eurasia collision, which caused uplift of the Tibetan plateau less than 50 Mys. ago (Mattauer et al., 1992; Burg et al., 1995; Ratschbacher et al., 1996; Rowley, 1996; Rowley, 1998; Yin and Harrison, 2000). The collision may have produced sinistral strike-slip faulting and eastward extrusion of the Tibetan plateau (Tapponnier et al., 1982) and affected the whole Tibetan plateau, including the Longmenshan thrust belt (Dirks et al., 1994; Chen and Wilson, 1996; Arne et al., 1997). The $^{40}Ar/^{39}Ar$ cooling ages in Danba, which are scattered between 47 and 81 Ma, suggest a substantially thickened crust even before the India-Eurasia collision. The slow cooling history shown by the large age discrepancies in Danba is in contrast to the fast cooling process in Longmenshan (Dirks et al., 1994; Chen and Wilson, 1996; Arne et al., 1997).

7. Conclusions

$^{40}Ar/^{39}Ar$ data demonstrate that there were three major tectono-thermal events in the Danba area, eastern margin of the Tibetan plateau. The Paleozoic cover sequence was metamorphosed to upper greenschist to lower amphibolite facies at 259–263 Ma, likely associated with underplating of the crust by mafic magma from the Emeishan mantle plume. The Neoproterozoic crystalline basement was first exhumed during 166–173 Ma, marking the beginning of a major period of extensional deformation in the region as a consequence of collision between the North China and South China blocks, and this extensional tectonics continued to 47–81 Ma, suggesting a progressive tectonic process. The wide age range of this thermal event reflects slow cooling in the area.

Acknowledgments

The work described in this paper was substantially supported by the National "973" Program of China (2007CB411401), and grants from the NSFC (Project 40621002), IRT0546, the 111 Project (No. B07011), and China Petroleum and Chemical Cooperation (CPCC09-01). We acknowledge an outstanding researcher award from Chinese Academy of Science (2005-2-21).

Appendix A

$^{40}Ar/^{39}Ar$ data of biotite and amphibole separates from the Danba domal terrane, eastern margin of the Tibetan plateau

Run ID#	Sample	$^{40}Ar/^{39}Ar$	$^{38}Ar/^{39}Ar$	$^{37}Ar/^{39}Ar$	$^{36}Ar/^{39}Ar$	$^{40}Ar^{*}/^{39}Ar$	Age (Ma)	± (Ma)	J	Er J	^{40}Ar (nA)	^{40}Ar (moles)	Laser (W)	Mineral	Heating (s)	Discr.	Er Discr.
1808-01A	GZ-2	7.91	1.60E−02	0.00E+00	−2.51E−02	1.53E+01	99.11	8.29	0.003684	0.000003	0.03	1.18E−15	0.20	Biotite	46.92	1.0169	0.0017
1808-01B	GZ-2	7.39	1.40E−02	0.00E+00	−7.46E−04	7.61E+00	49.87	3.32	0.003684	0.000003	0.07	3.00E−15	0.30	Biotite	46.90	1.0169	0.0017
1808-01C	GZ-2	7.52	1.53E−02	0.00E+00	−5.45E−04	7.68E+00	50.35	3.12	0.003684	0.000003	0.08	3.17E−15	0.40	Biotite	46.73	1.0169	0.0017
1808-01D	GZ-2	7.23	1.70E−02	0.00E+00	1.01E−03	6.93E+00	45.51	3.39	0.003684	0.000003	0.07	2.82E−15	0.50	Biotite	46.83	1.0169	0.0017
1808-01E	GZ-2	7.18	1.30E−02	0.00E+00	−2.78E−03	8.00E+00	52.40	3.08	0.003684	0.000003	0.08	3.25E−15	0.59	Biotite	46.83	1.0169	0.0017
1808-01F	GZ-2	7.42	1.33E−02	0.00E+00	1.81E−03	6.88E+00	45.18	1.51	0.003684	0.000003	0.16	6.64E−15	0.79	Biotite	46.93	1.0169	0.0017
1808-01G	GZ-2	7.82	1.34E−02	0.00E+00	7.11E−03	5.72E+00	37.61	3.81	0.003684	0.000003	0.07	2.78E−15	1.19	Biotite	47.00	1.0169	0.0017
1808-01H	GZ-2	6.65	1.23E−02	0.00E+00	6.69E−03	4.67E+00	30.78	4.70	0.003684	0.000003	0.04	1.83E−15	1.99	Biotite	46.93	1.0169	0.0017
1808-02A	GZ-2	9.81	1.07E−02	0.00E+00	8.10E−05	9.78E+00	63.87	3.74	0.003684	0.000003	0.08	3.32E−15	0.20	Biotite	46.85	1.0163	0.0017
1808-02B	GZ-2	9.16	1.12E−02	0.00E+00	4.79E−04	9.02E+00	58.95	1.68	0.003684	0.000003	0.18	7.37E−15	0.30	Biotite	46.87	1.0163	0.0017
1808-02C	GZ-2	9.14	1.22E−02	3.34E−01	−1.72E−05	9.17E+00	59.95	1.27	0.003684	0.000003	0.24	1.02E−14	0.40	Biotite	46.92	1.0163	0.0017
1808-02D	GZ-2	8.93	1.01E−02	6.48E−01	2.02E−03	8.38E+00	54.87	2.03	0.003684	0.000003	0.14	5.87E−15	0.50	Biotite	46.93	1.0163	0.0017
1808-02E	GZ-2	8.63	9.61E−03	0.00E+00	−5.56E−04	8.79E+00	57.49	3.03	0.003684	0.000003	0.10	4.26E−15	0.59	Biotite	46.88	1.0163	0.0017
1808-02F	GZ-2	8.16	1.01E−02	0.00E+00	2.16E−05	8.15E+00	53.40	2.77	0.003684	0.000003	0.09	3.82E−15	0.79	Biotite	46.72	1.0163	0.0017
1808-02G	GZ-2	8.11	1.43E−02	0.00E+00	−1.27E−03	8.49E+00	55.55	4.46	0.003684	0.000003	0.05	2.21E−15	1.19	Biotite	46.73	1.0163	0.0017
1808-02H	GZ-2	9.29	2.01E−02	0.00E+00	5.69E−03	7.61E+00	49.88	40.80	0.003684	0.000003	0.01	2.46E−16	1.99	Biotite	46.85	1.0163	0.0017
1808-03A	GZ-2	8.43	1.55E−02	1.01E−01	4.30E−03	7.17E+00	47.02	6.27	0.003684	0.000003	0.04	1.64E−15	0.20	Biotite	46.88	1.0163	0.0017
1808-03B	GZ-2	7.70	9.73E−03	0.00E+00	9.02E−04	7.43E+00	48.73	2.81	0.003684	0.000003	0.09	3.61E−15	0.30	Biotite	46.95	1.0163	0.0017
1808-03C	GZ-2	7.26	8.67E−03	3.02E−02	−5.44E−03	8.87E+00	58.02	3.77	0.003684	0.000003	0.06	2.65E−15	0.40	Biotite	46.77	1.0163	0.0017
1808-03D	GZ-2	7.25	1.13E−02	0.00E+00	2.79E−03	6.42E+00	42.18	3.11	0.003684	0.000003	0.07	3.11E−15	0.50	Biotite	46.68	1.0163	0.0017
1808-03E	GZ-2	7.18	9.87E−03	0.00E+00	−5.28E−04	7.34E+00	48.14	2.72	0.003684	0.000003	0.08	3.38E−15	0.59	Biotite	46.97	1.0163	0.0017
1808-03F	GZ-2	8.47	9.00E−03	0.00E+00	6.85E−03	6.44E+00	42.32	4.13	0.003684	0.000003	0.07	2.88E−15	0.80	Biotite	47.00	1.0163	0.0017
1808-03G	GZ-2	8.90	9.11E−03	0.00E+00	−8.18E−03	1.13E+01	73.68	9.03	0.003684	0.000003	0.03	1.30E−15	0.99	Biotite	46.95	1.0163	0.0017
1808-03H	GZ-2	9.95	2.63E−02	0.00E+00	−2.88E−02	1.84E+01	118.60	59.41	0.003684	0.000003	0.01	2.03E−16	1.19	Biotite	46.82	1.0163	0.0017
1808-03I	GZ-2	9.45	5.70E−03	0.00E+00	−4.31E−02	2.22E+01	141.77	28.11	0.003684	0.000003	0.01	4.04E−16	1.99	Biotite	46.65	1.0163	0.0017
1809-01A	GC-1	19.39	1.86E−02	0.00E+00	4.46E−02	6.20E+00	40.74	3.74	0.003684	0.000003	0.22	9.10E−15	0.20	Biotite	46.90	1.0163	0.0017
1809-01B	GC-1	14.39	1.48E−02	0.00E+00	1.39E−02	1.03E+01	67.07	0.74	0.003684	0.000003	1.55	6.41E−14	0.30	Biotite	46.83	1.0163	0.0017
1809-01C	GC-1	12.61	1.30E−02	0.00E+00	2.54E−03	1.19E+01	77.13	0.50	0.003684	0.000003	1.07	4.50E−14	0.40	Biotite	46.93	1.0163	0.0017
1809-01D	GC-1	12.22	1.35E−02	0.00E+00	2.20E−03	1.16E+01	75.33	0.81	0.003684	0.000003	0.56	2.35E−14	0.50	Biotite	46.93	1.0163	0.0017
1809-01E	GC-1	11.82	1.35E−02	0.00E+00	3.06E−03	1.09E+01	71.14	0.79	0.003684	0.000003	0.57	2.40E−14	0.69	Biotite	47.02	1.0163	0.0017
1809-01F	GC-1	11.42	1.31E−02	0.00E+00	1.96E−03	1.08E+01	70.66	1.44	0.003684	0.000003	0.27	1.12E−14	0.89	Biotite	46.87	1.0163	0.0017
1809-01G	GC-1	10.88	1.41E−02	0.00E+00	7.89E−04	1.06E+01	69.39	3.84	0.003684	0.000003	0.10	4.09E−15	1.19	Biotite	46.90	1.0163	0.0017
1809-01H	GC-1	11.57	1.30E−02	0.00E+00	4.48E−03	1.02E+01	66.83	3.17	0.003684	0.000003	0.13	5.25E−15	2.97	Biotite	46.38	1.0163	0.0017
1809-02A	GC-1	15.54	1.40E−02	1.65E−01	1.57E−02	1.09E+01	71.13	1.22	0.003684	0.000003	0.64	2.66E−14	0.20	Biotite	46.75	1.0163	0.0017
1809-02B	GC-1	12.90	1.29E−02	0.00E+00	3.25E−03	1.19E+01	77.66	0.61	0.003684	0.000003	0.89	3.74E−14	0.30	Biotite	46.80	1.0163	0.0017
1809-02C	GC-1	12.54	1.21E−02	0.00E+00	1.74E−03	1.20E+01	78.20	0.66	0.003684	0.000003	0.79	3.32E−14	0.40	Biotite	46.70	1.0163	0.0017
1809-02D	GC-1	12.57	1.29E−02	0.00E+00	−9.73E−06	1.26E+01	81.70	0.42	0.003684	0.000003	1.30	5.47E−14	0.50	Biotite	46.77	1.0163	0.0017
1809-02E	GC-1	12.59	1.22E−02	0.00E+00	2.97E−04	1.25E+01	81.23	0.32	0.003684	0.000003	1.99	8.36E−14	0.69	Biotite	46.83	1.0163	0.0017
1809-02F	GC-1	12.44	1.20E−02	0.00E+00	1.79E−04	1.24E+01	80.51	0.39	0.003684	0.000003	1.49	6.28E−14	0.89	Biotite	46.87	1.0163	0.0017
1809-02G	GC-1	12.54	1.26E−02	0.00E+00	9.69E−04	1.23E+01	79.65	0.39	0.003684	0.000003	1.40	5.90E−14	1.19	Biotite	46.90	1.0163	0.0017
1809-02H	GC-1	12.37	1.28E−02	0.00E+00	9.02E−04	1.21E+01	78.71	0.50	0.003684	0.000003	0.99	4.16E−14	2.97	Biotite	46.40	1.0163	0.0017
1809-03A	GC-1	11.70	1.43E−02	0.00E+00	1.76E−02	6.51E+00	42.74	3.73	0.003684	0.000003	0.11	4.45E−15	0.20	Biotite	46.82	1.0174	0.0019
1809-03B	GC-1	9.82	1.25E−02	1.09E−01	3.18E−03	8.89E+00	58.14	1.28	0.003684	0.000003	0.26	1.07E−14	0.30	Biotite	46.47	1.0174	0.0019
1809-03C	GC-1	10.04	1.22E−02	0.00E+00	1.01E−04	1.00E+01	65.33	0.79	0.003684	0.000003	0.47	1.99E−14	0.40	Biotite	46.82	1.0174	0.0019
1809-03D	GC-1	10.03	1.34E−02	0.00E+00	−3.53E−04	1.01E+01	66.12	0.85	0.003684	0.000003	0.43	1.82E−14	0.50	Biotite	46.67	1.0174	0.0019
1809-03E	GC-1	9.95	1.29E−02	0.00E+00	1.13E−04	9.91E+00	64.71	0.70	0.003684	0.000003	0.52	2.18E−14	0.69	Biotite	46.85	1.0174	0.0019
1809-03F	GC-1	9.59	1.24E−02	0.00E+00	1.38E−04	9.54E+00	62.34	0.81	0.003684	0.000003	0.39	1.64E−14	0.89	Biotite	46.95	1.0174	0.0019
1809-03G	GC-1	9.60	1.29E−02	3.10E−02	−4.22E−04	9.73E+00	63.53	1.36	0.003684	0.000003	0.26	1.10E−14	1.19	Biotite	46.50	1.0174	0.0019
1809-03H	GC-1	9.60	1.23E−02	0.00E+00	−2.16E−03	1.02E+01	66.82	1.77	0.003684	0.000003	0.19	7.98E−15	2.97	Biotite	45.98	1.0174	0.0019
1812-03A	GZ-5	124.75	1.02E−02	3.46E+01	−3.64E−01	2.41E+02	1145.99	98.99	0.003684	0.000003	0.02	1.02E−15	0.20	Amphibole	46.73	1.0174	0.0019
1812-03B	GZ-5	23.21	−3.28E−02	0.00E+00	−2.08E−01	8.45E+01	489.12	229.83	0.003684	0.000003	0.00	1.03E−16	0.30	Amphibole	46.72	1.0174	0.0019
1812-03C	GZ-5	35.17	2.88E−02	0.00E+00	−1.40E−01	7.65E+01	448.05	138.83	0.003684	0.000003	0.01	2.55E−16	0.40	Amphibole	46.67	1.0174	0.0019
1812-03D	GZ-5	26.79	1.51E−02	0.00E+00	−2.87E−02	3.53E+01	220.46	33.10	0.003684	0.000003	0.02	9.58E−16	0.50	Amphibole	46.95	1.0174	0.0019

1812-03E	GZ-5	35.27	2.98E−02	6.84E+00	−2.71E−03	3.68E+01	229.24	15.71	0.003684	0.000003	0.07	2.81E−15	0.59	Amphibole	47.07	1.0174	0.0019
1812-03F	GZ-5	31.73	2.78E−02	1.05E+01	1.55E−02	2.82E+01	178.10	11.64	0.003684	0.000003	0.08	3.50E−15	0.64	Amphibole	46.87	1.0174	0.0019
1812-03G	GZ-5	30.61	1.73E−02	1.01E+01	8.73E−03	2.90E+01	183.28	6.98	0.003684	0.000003	0.15	6.48E−15	0.69	Amphibole	46.93	1.0174	0.0019
1812-03H	GZ-5	25.64	2.55E−02	1.30E+01	1.50E−02	2.24E+01	143.21	8.70	0.003684	0.000003	0.09	3.89E−15	0.74	Amphibole	46.80	1.0174	0.0019
1812-03I	GZ-5	25.25	1.13E−02	1.17E+01	6.08E−03	2.46E+01	156.31	13.68	0.003684	0.000003	0.06	2.61E−15	0.79	Amphibole	46.65	1.0174	0.0019
1812-03J	GZ-5	26.20	1.51E−02	1.36E+01	1.79E−02	2.22E+01	141.77	16.79	0.003684	0.000003	0.05	2.06E−15	0.89	Amphibole	46.78	1.0174	0.0019
1812-03K	GZ-5	37.65	3.42E−02	2.31E+01	5.91E−02	2.24E+01	142.78	32.24	0.003684	0.000003	0.04	1.54E−15	1.18	Amphibole	46.85	1.0174	0.0019
1812-03L	GZ-5	35.63	1.45E−02	1.48E+01	1.95E−03	3.66E+01	228.13	11.08	0.003684	0.000003	0.11	4.63E−15	1.99	Amphibole	46.53	1.0174	0.0019
1814-01A	GZ-9	10.92	1.65E−02	0.00E+00	1.13E−02	7.59E+00	49.76	2.70	0.003684	0.000003	0.15	6.25E−15	0.20	Biotite	46.97	1.0167	0.0018
1814-01B	GZ-9	9.27	1.43E−02	0.00E+00	3.23E−03	8.31E+00	54.41	1.99	0.003684	0.000003	0.15	6.42E−15	0.30	Biotite	47.07	1.0167	0.0018
1814-01C	GZ-9	8.99	1.18E−02	0.00E+00	4.50E−03	7.66E+00	50.20	2.93	0.003684	0.000003	0.10	4.40E−15	0.40	Biotite	46.82	1.0167	0.0018
1814-01D	GZ-9	8.86	1.19E−02	2.49E−01	5.10E−03	7.38E+00	48.37	2.63	0.003684	0.000003	0.12	4.85E−15	0.50	Biotite	46.65	1.0167	0.0018
1814-01E	GZ-9	8.97	1.42E−02	4.12E−01	2.78E−03	8.18E+00	53.58	1.46	0.003684	0.000003	0.18	7.75E−15	0.69	Biotite	47.05	1.0167	0.0018
1814-01F	GZ-9	8.93	1.63E−02	0.00E+00	8.47E−03	6.43E+00	42.25	4.53	0.003684	0.000003	0.06	2.47E−15	0.89	Biotite	46.87	1.0167	0.0018
1814-01G	GZ-9	8.70	3.39E−02	0.00E+00	−1.68E−02	1.37E+01	88.67	44.02	0.003684	0.000003	0.01	2.41E−16	1.19	Biotite	46.98	1.0167	0.0018
1814-01H	GZ-9	8.70	3.22E−02	8.71E+00	3.25E−02	−2.38E−01	−1.58	40.54	0.003684	0.000003	0.01	2.79E−16	1.99	Biotite	47.02	1.0167	0.0018
1814-02A	GZ-9	11.11	1.12E−02	0.00E+00	7.29E−03	8.96E+00	58.58	1.44	0.003684	0.000003	0.32	1.33E−14	0.20	Biotite	46.65	1.0167	0.0018
1814-02B	GZ-9	9.21	1.18E−02	3.35E−03	1.75E−03	8.69E+00	56.86	0.74	0.003684	0.000003	0.44	1.82E−14	0.30	Biotite	46.82	1.0167	0.0018
1814-02C	GZ-9	9.02	1.34E−02	0.00E+00	1.25E−03	8.65E+00	56.57	0.85	0.003684	0.000003	0.36	1.52E−14	0.40	Biotite	46.63	1.0167	0.0018
1814-02D	GZ-9	9.00	1.10E−02	0.00E+00	1.72E−03	8.49E+00	55.57	1.09	0.003684	0.000003	0.30	1.28E−14	0.50	Biotite	47.07	1.0167	0.0018
1814-02E	GZ-9	8.94	1.25E−02	1.88E−01	1.00E−03	8.66E+00	56.65	0.68	0.003684	0.000003	0.48	2.00E−14	0.69	Biotite	46.95	1.0167	0.0018
1814-02F	GZ-9	9.00	1.23E−02	0.00E+00	2.07E−03	8.39E+00	54.89	1.00	0.003684	0.000003	0.33	1.40E−14	0.89	Biotite	46.92	1.0167	0.0018
1814-02G	GZ-9	8.95	1.29E−02	0.00E+00	4.09E−03	7.74E+00	50.69	2.29	0.003684	0.000003	0.13	5.41E−15	1.19	Biotite	46.80	1.0167	0.0018
1814-02H	GZ-9	8.59	5.18E−03	7.39E+00	1.92E−02	3.51E+00	23.19	12.92	0.003684	0.000003	0.02	8.53E−16	1.99	Biotite	46.97	1.0167	0.0018
1814-03A	GZ-9	15.46	2.01E−02	1.45E+00	2.87E−02	7.09E+00	46.50	3.87	0.003684	0.000003	0.16	6.54E−15	0.20	Biotite	46.75	1.0167	0.0018
1814-03B	GZ-9	8.66	1.45E−02	5.00E−01	6.10E−03	6.89E+00	45.25	1.36	0.003684	0.000003	0.23	9.61E−15	0.30	Biotite	47.02	1.0167	0.0018
1814-03C	GZ-9	8.30	1.27E−02	3.38E−01	2.40E−03	7.62E+00	49.96	1.67	0.003684	0.000003	0.18	7.45E−15	0.40	Biotite	47.00	1.0167	0.0018
1814-03D	GZ-9	8.37	1.03E−02	0.00E+00	2.96E−03	7.50E+00	49.14	1.63	0.003684	0.000003	0.17	7.30E−15	0.50	Biotite	46.78	1.0167	0.0018
1814-03E	GZ-9	8.54	1.26E−02	0.00E+00	1.31E−03	8.15E+00	53.39	1.69	0.003684	0.000003	0.18	7.49E−15	0.59	Biotite	46.57	1.0167	0.0018
1814-03F	GZ-9	8.42	1.49E−02	1.10E−01	2.19E−03	7.78E+00	51.01	1.81	0.003684	0.000003	0.16	6.61E−15	0.69	Biotite	46.93	1.0167	0.0018
1814-03G	GZ-9	8.46	1.23E−02	0.00E+00	9.34E−04	8.18E+00	53.57	1.59	0.003684	0.000003	0.18	7.44E−15	0.89	Biotite	46.65	1.0167	0.0018
1814-03H	GZ-9	8.51	1.36E−02	0.00E+00	4.60E−03	7.15E+00	46.87	3.22	0.003684	0.000003	0.08	3.18E−15	1.19	Biotite	47.10	1.0167	0.0018
1814-03I	GZ-9	8.38	2.30E−02	3.58E−01	3.41E−02	−1.66E+00	−11.04	15.23	0.003684	0.000003	0.02	6.36E−16	1.99	Biotite	46.95	1.0167	0.0018
1815-01A	DB-6	40.72	1.75E−02	0.00E+00	1.50E−02	3.63E+01	226.38	5.31	0.003684	0.000003	0.27	1.13E−14	0.20	Biotite	47.28	1.0167	0.0018
1815-01B	DB-6	41.96	1.31E−02	0.00E+00	2.48E−03	4.12E+01	255.10	1.00	0.003684	0.000003	3.00	1.26E−13	0.30	Biotite	46.82	1.0167	0.0018
1815-01C	DB-6	42.14	1.24E−02	0.00E+00	1.02E−03	4.18E+01	258.62	0.80	0.003684	0.000003	4.05	1.71E−13	0.40	Biotite	46.97	1.0167	0.0018
1815-01D	DB-6	42.33	1.17E−02	0.00E+00	1.25E−03	4.20E+01	259.31	0.87	0.003684	0.000003	2.98	1.26E−13	0.50	Biotite	46.77	1.0167	0.0018
1815-01E	DB-6	42.18	1.25E−02	0.00E+00	8.35E−04	4.19E+01	259.18	0.71	0.003684	0.000003	5.26	2.21E−13	0.69	Biotite	47.03	1.0167	0.0018
1815-01F	DB-6	42.04	1.20E−02	0.00E+00	9.05E−04	4.18E+01	258.22	0.69	0.003684	0.000003	5.74	2.42E−13	0.89	Biotite	47.03	1.0167	0.0018
1815-01G	DB-6	42.10	1.19E−02	5.56E−03	1.27E−03	4.17E+01	257.95	0.74	0.003684	0.000003	4.10	1.73E−13	1.18	Biotite	47.10	1.0167	0.0018
1815-01H	DB-6	42.33	1.12E−02	0.00E+00	7.67E−03	4.01E+01	248.33	4.07	0.003684	0.000003	0.32	1.34E−14	1.98	Biotite	46.92	1.0167	0.0018
1815-02A	DB-6	25.90	1.92E−02	0.00E+00	3.47E−02	1.57E+01	101.17	1.61	0.003684	0.000003	1.17	4.86E−14	0.20	Biotite	46.95	1.0159	0.0018
1815-02B	DB-6	29.85	1.41E−02	2.71E−02	1.62E−02	2.51E+01	159.34	1.02	0.003684	0.000003	2.81	1.18E−13	0.30	Biotite	46.87	1.0159	0.0018
1815-02C	DB-6	32.97	1.44E−02	0.00E+00	1.26E−02	2.92E+01	184.51	0.84	0.003684	0.000003	2.66	1.11E−13	0.40	Biotite	47.08	1.0159	0.0018
1815-02D	DB-6	34.44	1.48E−02	6.91E−02	1.02E−02	3.14E+01	197.62	1.07	0.003684	0.000003	1.62	6.82E−14	0.50	Biotite	47.07	1.0159	0.0018
1815-02E	DB-6	35.10	1.44E−02	0.00E+00	1.10E−02	3.19E+01	200.21	0.85	0.003684	0.000003	2.77	1.17E−13	0.69	Biotite	46.67	1.0159	0.0018
1815-02F	DB-6	34.72	1.54E−02	0.00E+00	1.25E−02	3.10E+01	195.18	1.10	0.003684	0.000003	1.48	6.25E−14	0.89	Biotite	46.98	1.0159	0.0018
1815-02G	DB-6	33.06	1.48E−02	0.00E+00	1.48E−02	2.87E+01	181.34	1.93	0.003684	0.000003	0.66	2.78E−14	1.19	Biotite	46.68	1.0159	0.0018
1815-02H	DB-6	33.78	2.18E−02	0.00E+00	1.98E−02	2.79E+01	176.70	11.89	0.003684	0.000003	0.08	3.49E−15	1.99	Biotite	46.95	1.0159	0.0018
1816-01A	DB-8	51.10	2.17E−02	0.00E+00	7.98E−02	2.75E+01	174.11	10.40	0.003684	0.000003	0.19	7.94E−15	0.20	Amphibole	47.17	1.0159	0.0018
1816-01B	DB-8	43.23	1.33E−02	1.17E−01	4.71E−03	4.18E+01	258.66	0.97	0.003684	0.000003	2.72	1.15E−13	0.30	Amphibole	46.53	1.0159	0.0018
1816-01C	DB-8	43.00	1.20E−02	7.29E−04	6.31E−04	4.28E+01	264.19	0.77	0.003684	0.000003	4.87	2.05E−13	0.40	Amphibole	46.57	1.0159	0.0018
1816-01D	DB-8	43.04	1.25E−02	4.05E−02	9.70E−04	4.28E+01	263.91	0.75	0.003684	0.000003	5.62	2.37E−13	0.59	Amphibole	46.82	1.0159	0.0018
1816-01E	DB-8	42.92	1.24E−02	8.64E−02	6.78E−04	4.27E+01	263.75	0.66	0.003684	0.000003	6.67	2.81E−13	0.79	Amphibole	46.77	1.0159	0.0018
1816-01F	DB-8	42.62	1.34E−02	5.24E−02	1.68E−03	4.21E+01	260.29	1.14	0.003684	0.000003	1.80	7.57E−14	0.99	Amphibole	47.07	1.0159	0.0018
1816-01G	DB-8	38.51	5.20E−02	1.83E−01	9.25E−03	3.58E+01	223.49	15.51	0.003684	0.000003	0.07	3.31E−15	1.19	Amphibole	47.02	1.0159	0.0018
1816-01H	DB-8	38.35	1.64E−02	0.00E+00	7.30E−03	3.62E+01	225.80	8.47	0.003684	0.000003	0.14	6.06E−15	1.98	Amphibole	46.88	1.0159	0.0018

(*continued on next page*)

Appendix A (*continued*)

Run ID#	Sample	$^{40}Ar/^{39}Ar$	$^{38}Ar/^{39}Ar$	$^{37}Ar/^{39}Ar$	$^{36}Ar/^{39}Ar$	$^{40}Ar^{*}/^{39}Ar$	Age (Ma)	± (Ma)	J	Er J	^{40}Ar (nA)	^{40}Ar (moles)	Laser (W)	Mineral	Heating (s)	Discr.	Er Discr.
1816-02A	DB-8	−20603.99	−7.50E−01	3.26E+02	1.08E+01	−3.09E+04	0.00	5233.02	0.003684	0.000003	0.11	4.60E−15	0.20	Amphibole	46.90	1.0159	0.0018
1816-02B	DB-8	1970.38	−2.37E−01	4.24E+02	−2.14E+00	3.76E+03	4867.70	2008.91	0.003684	0.000003	0.02	9.01E−16	0.30	Amphibole	46.82	1.0159	0.0018
1816-02C	DB-8	91.01	2.54E−01	1.89E+02	−7.54E−02	1.48E+02	784.16	385.77	0.003684	0.000003	0.01	2.53E−16	0.40	Amphibole	46.82	1.0159	0.0018
1816-02D	DB-8	25.28	1.42E−02	3.74E+01	6.28E−03	2.71E+01	171.42	11.31	0.003684	0.000003	0.07	2.91E−15	0.59	Amphibole	46.95	1.0159	0.0018
1816-02E	DB-8	24.48	1.75E−02	2.66E+01	1.24E−02	2.33E+01	148.79	10.36	0.003684	0.000003	0.08	3.16E−15	0.79	Amphibole	47.02	1.0159	0.0018
1816-02F	DB-8	53.23	−3.39E−01	6.63E+01	−4.73E−01	2.08E+02	1025.26	279.50	0.003684	0.000003	0.00	1.66E−16	0.99	Amphibole	46.73	1.0159	0.0018
1816-02G	DB-8	160.28	−8.00E−01	2.08E+02	−4.45E+00	1.75E+03	3619.41	1014.58	0.003684	0.000003	0.00	1.32E−16	1.19	Amphibole	47.03	1.0159	0.0018
1816-02H	DB-8	16.16	−3.93E−01	1.08E+02	−1.46E+00	4.92E+02	1866.05	298.90	0.003684	0.000003	0.00	3.69E−17	1.99	Amphibole	46.78	1.0159	0.0018

References

Ali, J.R., Lo, C.-H., Thompson, G.M., Song, X.Y., 2004. Emeishan basalt Ar–Ar overprint ages define several tectonic events that affected the western Yangtze platform in the Mesozoic and Cenozoic. Journal of Asian Earth Sciences 23, 163–178.

Arne, D., Worley, B., Wilson, C., Chen, S.F., Foster, D., Luo, Z.L., Liu, S.G., Dirks, P., 1997. Differential exhumation in response to episodic thrusting along the eastern margin of the Tibetan Plateau. Tectonophysics 280, 239–256.

Bodorkos, S., Sandiford, M., Oliver, N.H.S., Cawood, P.A., 2002. High-T, low-P metamorphism in the Palaeoproterozoic Halls Creek Orogen, northern Australia: the middle crustal response to a mantle-related transient thermal pulse. Journal of Metamorphic Geology 20, 217–237.

Boven, A., Pasteelsa, A.P., Punzalana, L.E., Liu, B.J., Luoa, X., Zhang, B.W., Guo, B.Z., Hertogen, C.J., 2002. $^{40}Ar/^{39}Ar$ geochronological constraints on the age and evolution of the Permo-Triassic Emeishan Volcanic Province, Southwest China. Journal of Asian Earth Sciences 20, 157–175.

Bruguier, O., Lancelot, J.R., Malavieille, J., 1997. U–Pb dating on single detrital zircon granites from the Triassic Songpan-Ganze flysch (Central China); provenance and tectonic correlations. Earth and Planetary Science Letters 152, 217–231.

Burchfiel, B.C., Chen, Z., Liu, Y., Royden, L.H., 1995. Tectonics of the Longmenshan and adjacent regions, central China. International Geological Review 37, 661–736.

Burchfiel, B.C., Molnar, P., Zhao, Z., Liang, K., Wang, S., Huang, J.F., Sutter, J.F., 1989. Geology of the Ulugh Muztagh area, northern Tibet. Earth and Planetary Science Letters 94, 57–70.

Burg, J.P., Davy, P., Martinod, J., 1995. Shortening of analogue models of the continental lithosphere: new hypothesis for the formation of the Tibetan plateau. Tectonics 13, 475–483.

Castonguay, S., Ruffet, G., Tremblay, A., Féraud, G., 2001. Tectono-metamorphic evolution of the southern Quebec Appalachians: $^{40}Ar/^{39}Ar$ evidence for Middle Ordovician crustal thickening and Silurian–Early Devonian exhumation of the internal Humber zone. Geological Society of America Bulletin 113, 144–160.

Chang, E.Z., 2000. Geology and tectonics of the Songpan-Ganze fold belt, Southwestern China. International Geology Review 42, 813–831.

Chen, S.F., Wilson, C.J.L., Worley, B.A., 1995. Tectonic transition from the Songpan-Ganze fold belt to the Sichuan basin, south-western China. Basin Research 7, 235–253.

Chen, S.F., Wilson, C.J.L., 1996. Emplacement of the Longmenshan Thrust-Nappe belt along the eastern margin of the Tibetan Plateau. Journal of Structural Geology 18, 413–430.

Chung, S.L., Jahn, B.M., 1995. Plume-lithosphere interaction in generation of the Emeishan flood basalts at the Permian–Triassic boundary. Geology 23, 889–892.

Collins, W.J., Vernon, R.H., 1994. A rift drift delamination model of continental evolution – paleozoic tectonic development of eastern Australia. Tectonophysics 235, 249–275.

Cosca, A., Hunziker, J.C., Huon, S., Masson, H., 1992. Radiometric age constraints on mineral growth, metamorphism, and tectonism in the Gumfluh Klippe, Briançonnais domain of the Préalpes, Switzerland. Contributions to Mineralogy and Petrology 112, 439–449.

Dewey, J.F., Shackleton, R.M., Chang, C.F., Sun, Y.Y., 1988. The tectonic evolution of the Tibetan Plateau. Philosophical Transactions of the Royal Society London A 327, 379–413.

Dirks, P.H.G.M., Wilson, C.J.L., Chen, S., Luo, Z.L., Liu, S., 1994. Tectonic evolution of the NE margin of the Tibetan Plateau, evidence from the central Longmen mountains, Sichuan province, China. Journal of Southeast Asian Earth Sciences 9, 181–192.

Guo, F., Fan, W.-M., Wang, Y., Li, C., 2004. When did the Emeishan mantle plume activity start? Geochronological and geochemical evidence from ultramafic-mafic dikes in Southwestern China. International Geology Review 46, 226–234.

He, B., Xu, Y.G., Chung, S.L., Xiao, L., Wang, Y., 2003. Sedimentary evidence for a rapid, kilometer-scale crustal doming prior to the eruption of the Emeishan flood basalts. Earth and Planetary Science Letters 213, 391–405.

Hess, J.C., Lippolt, H.J., Gurbanov, A.G., Michalski, I., 1993. The cooling history of the late Pliocene Eldzhurtinskiy granite (Caucasus, Russia) and the thermochronological potential of grain-size/age relationships. Earth and Planetary Science Letters 117, 393–406.

Hou, L.W., 1996. Type and genesis of domal deformational-metamorphic terranes in the western margin of the Yangtze craton. In: Luo, Y.N. (Ed.), Contributions to Geology and Mineral Resources in an Intracontinental Orogenic Belt on Southwestern Margin of the Yangtze Block. Sichuan Science and Technology Press, Chengdu, China, pp. 13–27 (in Chinese).

Hou, Z.Q., Chen, W., Lu, J.R., 2002. Collision event during 177–135 Ma on the eastern margin of the Qinghai-Tibet plateau: evidence from Ar–Ar dating for basalts on the western margin of the Yangtze platform. Acta Geological Sinica – English Edition 76, 194–204.

Huang, M.H., Hou, L.W., Fu, X.F., 1996. P-T-t-D Path of metamorphic terranes in the Danba area. In: Luo, Y.N. (Ed.), Contributions to Geology Mineral Resources in an Intracontinental Orogenic belt on the SW Margin of the Yangtze Block. Sichuan Science and Technology Press, Chengdu, China, pp. 41–50 (in Chinese).

Huang, M.H., Buick, I.S., Hou, L.W., 2003a. Tectonometamorphic evolution of the Eastern Tibet plateau: evidence from the central Songpan-Ganze orogenic belt, western China. Journal of Petrology 44, 255–278.

Huang, M., Maas, R., Buick, I.S., Williams, I.S., 2003b. Crustal response to continental collisions between the Tibet, Indian, South China and North China blocks: geochronological constraints from the Songpan-Ganze Orogenic Belt, Western China. Journal of Metamorphic Geology 21, 223–240.

Kirby, E., Reiners, P.W., Krol, M.A., Whipple, K.X., Hodges, K.V., Farley, K.A., Tang, W.Q., Chen, Z.L., 2002. Late Cenozoic evolution of the eastern margin of the Tibetan Plateau: inferences from $^{40}Ar/^{39}Ar$ and (U–Th)/He thermochronology. Tectonics 21, 3–22.

Li, S., Chen, Y., Cong, B., Zhang, Z., Zhang, R., Liou, D., Hart, S.R., Ge, N., 1993. Collision of the North China and the Yangtze blocks and formation of coesite-bearing eclogites: timing and processes. Chemical Geology 109, 70–89.

Li, Z.X., Metcalfe, I., Wang, X.F., 1995. Vertical-axis block rotations in southwestern China since the Cretaceous – new paleomagnetic results from Hainan-island. Geophysical Research Letters 22, 3071–3074.

Liu, H.F., Lian, H.S., Cai, L.G., Shen, F., 1994. Structural styles of the Longmenshan thrust belt and evolution of the foreland basin in the western Sichuan Province, China. Acta Geologica Sinica 68, 101–118 (in Chinese).

Markley, M.J., Teyssier, C., Cosca, M.A., Caby, R., Hunziker, J.C., Sartori, M., 1998. Alpine deformation and Ar-40/Ar-39 geochronology of synkinematic white mica in the Siviez-Mischabel Nappe, western Pennine Alps, Switzerland. Tectonics 17, 407–425.

Markley, M.J., Teyssier, C., Cosca, M., 2002. The relation between grain size and Ar-40/Ar-49 date for Alpine white mica from the Siviez-Mischabel Nappe, Switzerland. Journal of Structural Geology 24, 1937–1955.

Mattauer, M., Malavieille, J., Calassou, S., Lancelot, J., Roger, F., Hao, Z.W., Xu, Z.Q., Hou, L.W., 1992. The Songpan-Ganze Triassic belt of west Sichuan and eastern Tibet – a decollement fold belt on passive margin. Comptes Rendus de l' Academie des Sciences, Paris, II 314, 619–626.

McDougall, I., Harrison, T.M., 1999. Geochronology and Thermochronology by the $^{40}Ar/^{39}Ar$ Method. Oxford University Press, Oxford. 261 p.

Nie, S., Yin, A., Rowley, D.B., Jin, Y., 1994. Exhumation of the Dabie Shan ultra-high-pressure rocks and accumulation of the Songpan Ganze flysch sequence, central China. Geology 22, 999–1002.

Rao, R., Xu, J., Chen, Y., Zou, D., 1987. The Triassic System of the Qianghai-Xizang Plateau. Geological Publishing House, Beijing. 239 p.

Ratschbacher, L., Frisch, W., Chen, C., Pan, G., 1996. Cenozoic deformation, rotation, and stress patterns in eastern Tibet and western Sichuan, China. In: Yin, A., Harrison, T.M. (Eds.), The Tectonic Evolution of Asia. Cambridge University Press, New York, pp. 227–249.

Renne, P.R., Swisher, C.C., Deino, A.L., Karner, D.B., Owens, T.L., DePaolo, D.J., 1998. Intercalibration of standards, absolute ages and uncertainties in $^{40}Ar/^{39}Ar$ dating. Chemical Geology 145, 117–152.

Roger, F., Malavieille, J., Leloup, P., Calassou, S., Xu, Z., 2004. Timing of granite emplacement and cooling in the Songpan-Ganze fold belt (eastern Tibetan Plateau) with tectonic implications. Journal of Asian Earth Sciences 22, 465–481.

Roger, F., Calassou, S., 1997. U–Pb geochronology on zircon and isotope geochemistry (Pb, Sr, and Nd) of the basement in the Songpan-Garze fold belt (China). Comptes Rendus de l' Academie des Sciences, Paris, II 324, 819–826.

Rowley, D.B., 1996. Age of initiation of collision between India and Asia: a review of stratigraphic data. Earth and Planetary Science Letters 145, 1–13.

Rowley, D.B., 1998. Minimum age of initiation of collision between India and Asia north of Everest based on the subsidence history of the Zhepure Mountain section. Journal of Geology 106, 229–235.

Sandiford, M., Powell, R., 1986. Deep crustal metamorphism during continental extension; modern and ancient examples. Earth and Planetary Science Letters 79, 151–158.

Schmitz, M.D., Bowring, S.A., 2003. Ultrahigh-temperature metamorphism in the lower crust during Neoarchean Ventersdorp rifting and magmatism, Kaapvaal Craton, southern Africa. Geological Society of America Bulletin 115, 533–548.

SBGMR (Sichuan Bureau of Geology and Mineral Resources), 1991. Regional geology of Sichuan Province: Beijing, China, Geological Publishing House, 680 p (in Chinese).

Song, X.-Y., Zhou, M.-F., Cao, Z.M., Sun, M., 2003. Ni–Cu–(PGE) magmatic sulfide deposits in the Yangliuping area, Permian Emeishan igneous province, SW China. Mineralium Deposita 38, 831–843.

Song, X.-Y., Zhou, M.-F., Cao, Z., Robinson, P.T., 2004. Late Permian rifting of the South China Craton caused the Emeishan mantle plume. Journal of Geological Society of London 161, 773–781.

Steiger, R.H., Jager, E., 1977. Subcommission on geochronology-convention on use of decay constants in geochronology and cosmochronology. Earth and Planetary Science Letters 36, 359–362.

Tapponnier, P., Peltzer, G., Le Dain, A.Y., Armijo, R., Cobbold, P., 1982. Propagating extrusion tectonics in Asia: new insights from simple experiments with plasticine. Geology 10, 611–616.

Vasconcelos, P.M., 1999. $^{40}Ar/^{39}Ar$ geochronology of supergene process in ore deposits. Reviews in Economic Geology 12, 73–113.

Wallis, S., Tsujimori, T., Aoya, M., Kawakami, T., Terada, K., Suzuki, K., Hyodo, H., 2003. Cenozoic and Mesozoic metamorphism in the Longmenshan orogen: implications for geodynamic models of eastern Tibet. Geology 31, 745–748.

Wang, E., Burchfiel, B.C., 2000. Late Cenozoic to Holocene deformation in southwestern Sichuan and adjacent Yunnan, China, and its role in formation of the southeastern part of the Tibetan Plateau. Geological Society of America Bulletin 112, 413–423.

West, P., Lux, D.R., 1993. Dating mylonitic deformation by the $^{40}Ar/^{39}Ar$ method; an example from the Norumbega fault zone, Maine. Earth and Planetary Science Letters 120, 221–237.

Wichham, S.M., Oxburgh, E.R., 1985. Continental rifts as a setting for regional metamorphism. Nature 318, 330–333.

Worley, B.A., Wilson, C.J.L., 1996. Deformation partitioning and foliation reactivation during transpressional orogenesis, an example from the central Longmen Shan, China. Journal of Structural Geology 18, 395–411.

Wright, N., Layer, P.W., York, D., 1991. New insights into thermal history from single grain $^{40}Ar/^{39}Ar$ analysis of biotite. Earth and Planetary Science Letters 104, 70–79.

Xia, Z.S., 1993. Syntectonic regional epimetamorphism of the Triassic terrigenous detrital rocks in the Songpan-Ganze orogneic belt during the early Yanshanian orogney. Acta Geologica Sichuan 13, 20–27 (in Chinese).

Xu, Z.Q., Hou, L.W., Wang, Z.X., 1992. Orogenic Processes of the Songpan-Garze Orogenic Belt of China. Geological Publisher House, Beijing, China. 137 p (in Chinese).

Yan, D.-P., Zhou, M.-F., Song, H., Fu, Z., 2003a. Structural Style and tectonic significance of the Jianglang dome in the Eastern Margin of the Tibetan Plateau, China. Journal of Structural Geology 25, 765–779.

Yan, D.-P., Zhou, M.-F., Song, H., Wang, X.-W., Malpas, J., 2003b. Origin and tectonic significance of a Mesozoic multi-layer over-thrust system within the Yangtze Block (South China). Tectonophysics 361, 239–254.

Yin, A., 2004. Gneiss domes and gneiss dome systems. In: Whitny, D.L., Teysser, C., Siddway, C.S. (Eds.), Gneiss Domes in Orogeny. Geological Society of America, Boulder Colorado, Special Paper 380, pp. 1–14.

Yin, A., Harrison, T.M., 2000. Geologic evolution of the Himalayan–Tibetan orogen. Annual Review of Earth and Planetary Sciences 28, 211–280.

Yin, A., Nie, S., 1993. An indentation model for North and South China collision and the development of the Tanlu and Honam fault systems, eastern Asia. Tectonics 12, 801–813.

Yin, A., Nie, S., 1996. A Phanerozoic palinspastic reconstruction of China and its neighboring region. In: Yin, A., Harrison, T.M. (Eds.), The Tectonic Evolution of Asia. Cambridge University Press, New York, pp. 442–485.

Zen, E.A., 1995. Crustal magma generation and low-pressure high-temperature regional metamorphism in an extentional environment; possible application to the Lachlan belt. American Journal of Science 295, 851–874.

Zhang, Q.R., Piper, J.D.A., 1997. Paleomagnetic study of Neoproterozoic glacial rocks of the Yangtze Block: paleolatitude and configuration of South china in the Late Proterozoic supercontinent. Precambrian Research 85, 173–199.

Zhou, D., Graham, S.A., 1996. The Songpan-Ganzi complex of the western Qinling Shan as a Triassic remnant ocean basin. In: Yin, A., Harrison, T.M. (Eds.), The Tectonic Evolution of Asia. Cambridge University Press, New York, pp. 281–299.

Zhou, M.-F., Yan, D.P., Kennedy, A.K., Li, Y.Q., Ding, J., 2002a. SHRIMP zircon geochronological and geochemical evidence for Neo-proterozoic arc-related magmatism along the western margin of the Yangtze Block, South China. Earth and Planetary Science Letters 196, 51–67.

Zhou, M.-F., Yang, Z.X., Song, X.-Y., Lesher, C.M., Keays, R.R., 2002b. Magmatic Ni–Cu–(PGE) sulfide deposits in China. In: Cabri, L.J. (Ed.) The Geology, Geochemistry, Mineralogy, Mineral Beneficiation of the Platinum-Group Elements. Canadian Institute of Mining, Metallurgy and Petroleum, Special vol. 54, pp. 619–636.

Zhou, M.-F., Malpas, J., Song, X.-Y., Kennedy, A.K., Robinson, P.T., Sun, M., Lesher, C.M., Keays, R.R., 2002c. A temporal link between the Emeishan large igneous province (SW China) and the end-Guadalupian mass extinction. Earth and Planetary Science Letters 196, 113–122.